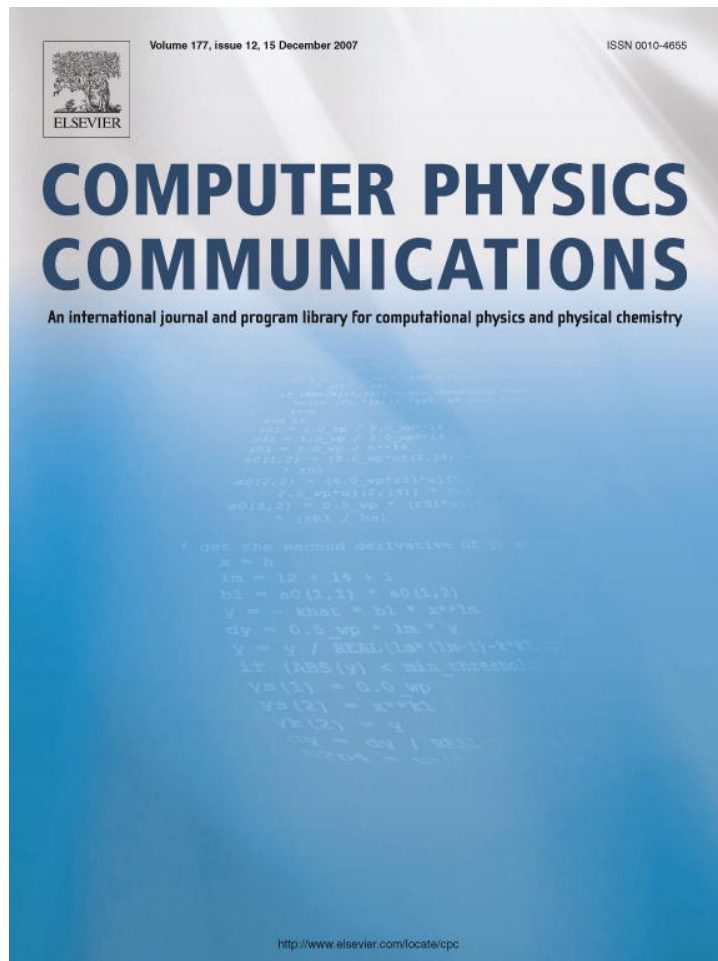


Provided for non-commercial research and education use.
Not for reproduction, distribution or commercial use.



This article was published in an Elsevier journal. The attached copy is furnished to the author for non-commercial research and education use, including for instruction at the author's institution, sharing with colleagues and providing to institution administration.

Other uses, including reproduction and distribution, or selling or licensing copies, or posting to personal, institutional or third party websites are prohibited.

In most cases authors are permitted to post their version of the article (e.g. in Word or Tex form) to their personal website or institutional repository. Authors requiring further information regarding Elsevier's archiving and manuscript policies are encouraged to visit:

<http://www.elsevier.com/copyright>



A numerical Maxwell–Schrödinger model for intense laser–matter interaction and propagation

E. Lorin^{a,b,*}, S. Chelkowski^c, A. Bandrauk^d

^a *Centre de Recherche en Mathématiques de Montréal, University of Montréal, Canada*

^b *University of Ontario, Institute of Technology, Oshawa, Canada*

^c *Université de Sherbrooke, laboratoire de chimie théorique, Canada*

^d *Université de Sherbrooke, laboratoire de chimie théorique, Centre de Recherche en Mathématiques de Montréal, Canada Research Chair, Canada*

Received 29 March 2007; accepted 21 July 2007

Available online 31 July 2007

Abstract

We present in this paper an original *ab initio* Maxwell–Schrödinger model and a methodology to simulate intense ultrashort laser pulses interacting with a 3D H_2^+ -gas in the nonlinear nonperturbative regime under and beyond Born–Oppenheimer approximation. The model we present is the first one to our knowledge (excepted in [E. Lorin, S. Chelkowski, A. Bandrauk, A Maxwell–Schrödinger model for non-perturbative laser–molecule interaction and some methods of numerical computation, Proceeding CRM, vol. 41, American Mathematics Society, 2007], where a one-dimensional version is presented) to be totally nonperturbative, vectorial and multidimensional, taking into account ionization, and high order nonlinearities going far beyond classical nonlinear Maxwell or Schrödinger models. After a presentation of the model and a short mathematical study, we examine some numerical approximations for its computation. In particular, we focus on the polarization computation allowing an efficient coupling between the Maxwell and time dependent Schrödinger equations (TDSE), and on an efficient parallelization. Examples of numerical computations of high order harmonic generation and of electric field propagation are presented for one molecule and up to 512, thus highlighting cooperative effects in harmonic generation at high order.

© 2007 Elsevier B.V. All rights reserved.

Keywords: Maxwell; Schrödinger; Laser; Multiscales problem

1. Introduction

From the theoretical point of view to the very practical point of view (controlled nuclear fusion [14] by inertial confinement, quantum dynamic imaging [5], attosecond pulse generation [11]), there exist numerous applications of ultrashort and intense laser pulses. Indeed current laser technology allows to create ultrashort pulses with intensities exceeding the internal electric fields of some molecules and atoms. For the hydrogen atom, the electronic period of circulation is 24.6 attoseconds (10^{-18} s) and the Coulomb field intensity I is equal to $cE^2/8\pi = 3 \times 10^{16}$ W/cm² where c is the velocity of light, corresponding to a laser intensity $E = 5 \times 10^{11}$ V/m⁻¹. Current laser intensities can reach around 10^{20} W/cm² with pulse durations of ~ 20 femtoseconds (20×10^{-15} s), see Fig. 1. This naturally leads to a possible electronic motion controlled by electric fields (see Fig. 2) with applications in quantum imaging or controlled nuclear fusion. The main goal of this work is to introduce a model to study high order nonlinear phenomena (Above Threshold Ionization (ATI), High Harmonics Generation (HHG), filamentation [30], etc.) obtained with very intense laser pulses interacting with molecules and to study their dynamics. HHG is one of these nonlinear phenomena that appears when the electric field is of same order as the Coulomb potential field. Such strong fields lead to ionization and harmonics are created by electron rescattering [6,19]. It is, moreover, the current source of coherent attosecond pulses [1,11]. A simple three step

* Corresponding author.

E-mail address: lorin@crm.umontreal.ca (E. Lorin).

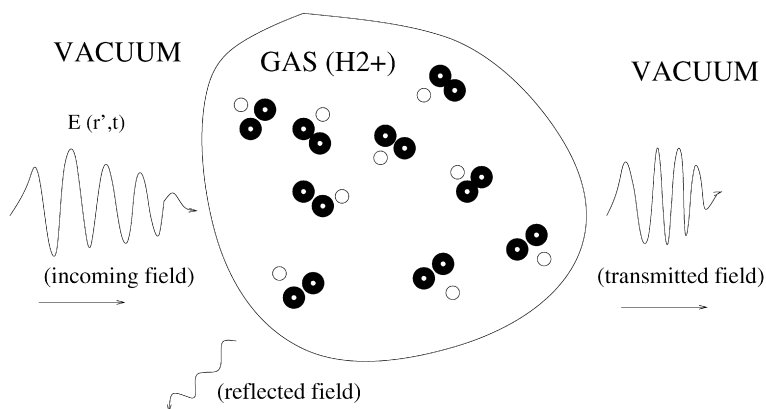


Fig. 1. Laser–matter interactions in a H_2^+ gas.

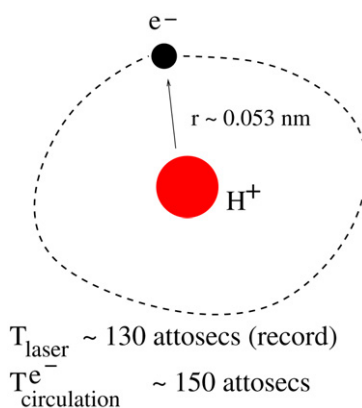


Fig. 2. Laser and electronic periods.

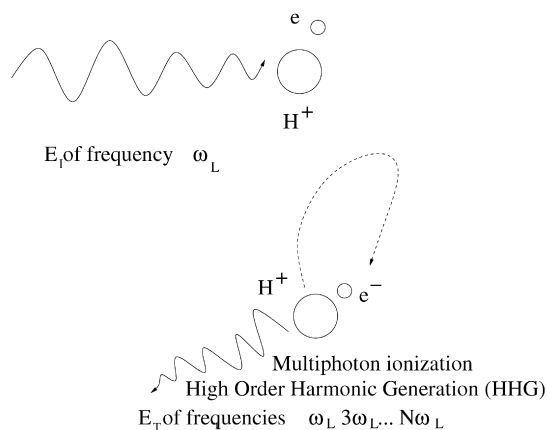


Fig. 3. High-order harmonic generation.

model allows to interpret the maximum energy $N\omega_L/2\pi$ of harmonics of order N created by an incoming laser field of frequency ω_L . In a first step excited by the intense electric field \mathbf{E}_I , the electron leaves the ion vicinity and enters the ionized continuum with an initial velocity equal to zero [6,19]. Then the free electron is accelerated by the strong electric field and gains energy. In a last step the electron is driven back into the vicinity of the parent ion and recombines with it, leading to further ionization (see [25] and [20]). As a consequence the transmitted electric field \mathbf{E}_T , possesses high order internal frequencies (see Figs. 3, 4). In this paper we will introduce a precise model to describe numerically the dynamics, including ionization, dissociation of the molecule and propagation effects in order to take into account phase matching [13] and collective multiparticle effects. Whereas previous works dealt with laser–atom interactions [13], we propose here to study ultrashort pulses interacting with molecules, in particular, we will focus on the one-electron H_2^+ -molecule [13]. The choice of H_2^+ -molecules is motivated by the fact that their quantum dynamics can be described exactly by a computable TDSE model (3 particles, but 2-body problem because of H_2^+ -symmetries). More sophisticated

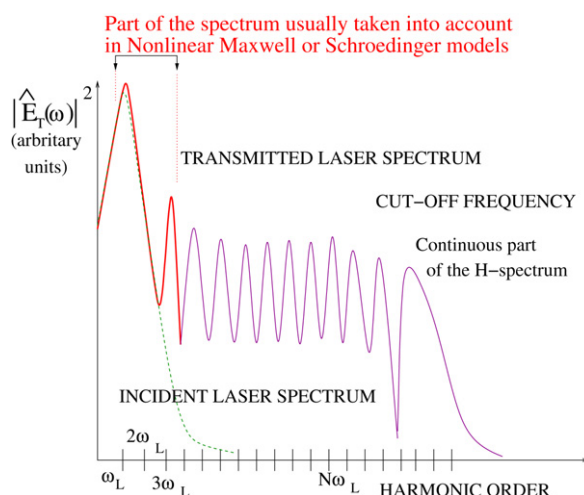
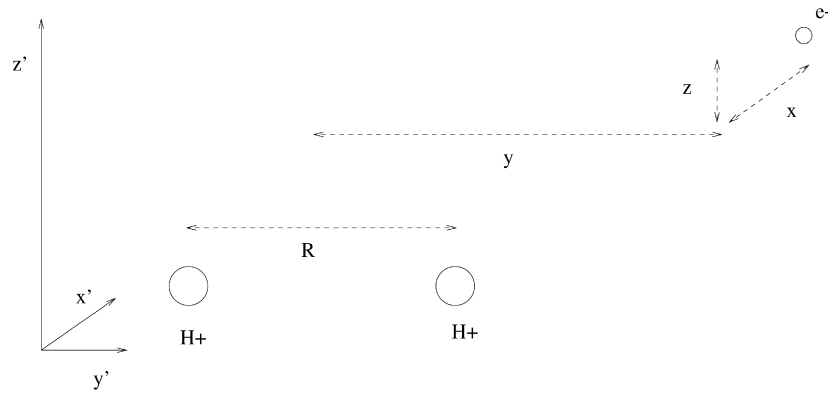


Fig. 4. Transmitted electric field spectrum.

molecules could of course be considered, but then some approximate models to describe their dynamics should be introduced to be numerically solved, such as Hartree–Fock, Kohn–Sham, Thomas–Fermi, TDDFT, etc. (see [28,29,38], for instance). At this point we want to have as much as possible a precise physical model, to describe the quantum dynamics and propagation of laser pulses. To model phase matching in molecular media such as propagation in the atmosphere [30], the most natural way is to consider a coupling between the Maxwell’s equations describing the behavior of the electric and magnetic fields, and the time dependent Schrödinger equation (TDSE) describing the quantum particle motions. In order to increase the precision of the model, we propose to go “beyond” the Born–Oppenheimer approximation which corresponds to static (zero velocity) nuclei (protons), taking into account the nuclear motions [15]. The Maxwell’s equations and the TDSE’s are then coupled with the polarization of molecules which depends on the relative position of the particles constituting the molecule. The model is written first in its whole generality and then some approximations are proposed in order to solve it numerically efficiently. The vectorial 3-D modeling we propose is to our knowledge the first one to present such a precision to model the intense and ultrashort laser–gas interactions. The simplest models to describe the electric field behavior in a medium are the nonlinear Schrödinger equations, based on slowly varying envelope and perturbative approximations. These models are then not able to capture high nonlinearities (beyond Kerr effects) and the ionization effects are totally neglected what is nonphysical for intense and ultrashort laser pulses. Other models such Maxwell–Bloch are also discussed in this paper but none of them is precise as the Maxwell–Schrödinger model. Note that the model we propose is close to the “one-dimensional” model presented in [16,17,32,33] but goes beyond as our approach is vectorial, three-dimensional and totally nonperturbative.

From a numerical point of view many difficulties arise from the model we present. First of all, numerous multiscales appear in the model due to the fact that the Maxwell’s equations we consider are macroscopic and that the TDSE describe microscopic motions. The time and space scales for the Maxwell’s equations are then much larger than the TDSE’s ones. However because of the molecular actions on the electric field, the internal electric field harmonics become larger and larger so that the range of time and space scales for the Maxwell’s equations increases. We then have to design our approach such that all multiscales can be captured at any time. This goal is even more difficult to reach because of additional constraints on the numerical time and space steps (for stability, convergence, accuracy). We discuss in this paper how to manage simultaneously both numerical and physical multiscale constraints. In order to solve the TDSE’s we propose to use a Crank–Nicolson finite difference scheme, stable and of order 2. As the laser intensities we consider are very high, the TDSE wavefunctions are delocalized. It is then necessary to impose some adapted boundary conditions to solve the TDSE in a sufficiently small numerical domain (recall that our approach is 3-D and then numerically very costly). In this aim some original boundary conditions will be proposed depending on the physical configuration. Commonly in the framework of laser–molecule interaction, absorbing boundary conditions are used. Even if they are very efficient to avoid usual numerical spurious reflections on the numerical domain boundaries, they unfortunately correspond to absorb some free electrons, whose effects are then totally lost.

Next, due to the number of the TDSE’s we have to solve in order to be able to precisely describe the gas effect on the electric and magnetic fields, an effective parallel approach is introduced again under important numerical and physical constraints. The approach we propose is based on the fact that the reaction of a sufficiently small elementary gas volume on the electric field can be described by one single TDSE. However to consider a sufficiently large volume of gas, it is necessary to solve numerous TDSE’s. Simultaneously the Maxwell’s equations and the TDSE’s are then solved in parallel. The coupling of these equations is ensured by the polarization that corresponds to the reaction of the gas on the electric field. The parallel technique we propose has a very good speed-up, and in the same time allows us to distribute very efficiently the numerical data in the super-computer memory.


 Fig. 5. Coordinates for the electric field \mathbf{E} , and electron wavefunction ψ .

The paper is organized as follows. Section 2 will be devoted to the presentation of our modeling and some existing models will be briefly discussed. Then we will focus on the existence of solutions for the TDSE's we consider. Section 3 will be devoted to the presentation of the general numerical method we have used to solve the coupled quantum field–particle system, using the Yee and Crank–Nicolson schemes. We will detail the polarization computation (and how to reduce its CPU cost) and will give some ideas on the multidimensional boundary conditions. The parallelization of the method for approximating Maxwell–Schrödinger will be presented in Section 4. In particular, we will demonstrate scalability as a function of number of H_2^+ -molecules. In the last Section 5 some numerical results will be presented in order to demonstrate effects of the field propagation, and multiparticle collective effects on HHG.

2. Model

2.1. Presentation of the Maxwell–Schrödinger model

The TDSE describing the H_2^+ -molecule behavior excited by a laser field in atomic units ($e = \hbar/2\pi = m_e = 1$, $c = 137$), can be written [20]:

$$i \partial_t \psi(\mathbf{r}, R, \mathbf{r}', t) = \left[-\frac{1}{2} \Delta_{\mathbf{r}} + V_c(\mathbf{r}, R) - \frac{i}{c} \mathbf{A}(\mathbf{r}', t) \cdot \nabla_{\mathbf{r}} + \frac{1}{R} - \frac{1}{m_p} \Delta_R + \frac{\|\mathbf{A}(\mathbf{r}', t)\|^2}{2c^2} \right] \psi(\mathbf{r}, R, \mathbf{r}', t), \quad (1)$$

where ψ represents the molecular wavefunction. Electron–nuclei and nuclear potential, V_c and V_i are given by

$$V_c(\mathbf{r}, R) = -\frac{1}{\sqrt{x^2 + (y - R/2)^2 + z^2}} - \frac{1}{\sqrt{x^2 + (y + R/2)^2 + z^2}}, \quad V_i(R) = \frac{1}{R}. \quad (2)$$

The electronic position in the nuclei center of mass coordinates is denoted by $\mathbf{r} = (x, y, z)^T$ (see Fig. 5). R represents the nuclear relative position and m_p ($m_p = 1837$ a.u.) denotes the H^+ mass. We suppose in this paper that the nuclear motion is one-dimensional. The variable \mathbf{r}' denotes the spatial dependence of the electric and magnetic fields, and \mathbf{A} represents the electromagnetic potential. Obviously the wavefunction depends on \mathbf{r}' . Note that in our orthogonal coordinates, we chose $\mathbf{e}_x = \mathbf{e}_{x'}$, $\mathbf{e}_y = \mathbf{e}_{y'}$, $\mathbf{e}_z = \mathbf{e}_{z'}$. Next, if the laser wavelength is large enough we can assume that the electric and magnetic fields are constant in space at the molecular scale $\lambda/\ell \gg 1$ (this corresponds to the dipole approximation [4,39]) allowing us to reduce the numerical and mathematical complexity of the problem. Indeed, in this situation the Schrödinger equation can be written:

$$i \partial_t \psi_{\mathbf{r}'}(\mathbf{r}, R, t) = \left[-\frac{1}{2} \Delta_{\mathbf{r}} + V_c(\mathbf{r}, R) - \frac{i}{c} \mathbf{A}_{\mathbf{r}'}(t) \cdot \nabla_{\mathbf{r}} + \frac{1}{R} - \frac{1}{m_p} \Delta_R + \frac{\|\mathbf{A}_{\mathbf{r}'}(t)\|^2}{2c^2} \right] \psi_{\mathbf{r}'}(\mathbf{r}, R, t), \quad (3)$$

\mathbf{r}' is now a parameter denoting the molecule position in the “Maxwell domain”. For each \mathbf{r}' in the gas, one has to solve a 4D-TDSE. Let us remark that this approximation leads to $[\Delta_{\mathbf{r}}, \mathbf{A}_{\mathbf{r}'}(t) \cdot \nabla_{\mathbf{r}}] = 0$; a very useful feature when a numerical splitting is applied.

The previous TDSE is given in the so-called *velocity gauge*. Another possible formulation is in the so-called *length gauge*. Applying the unitary transformation

$$\psi \mapsto \psi \exp\left(-\frac{i}{2c^2} \int_0^t \|\mathbf{A}_{\mathbf{r}'}\|^2(s) ds - \frac{i}{c} \mathbf{r} \cdot \mathbf{A}_{\mathbf{r}'}(t)\right), \quad (4)$$

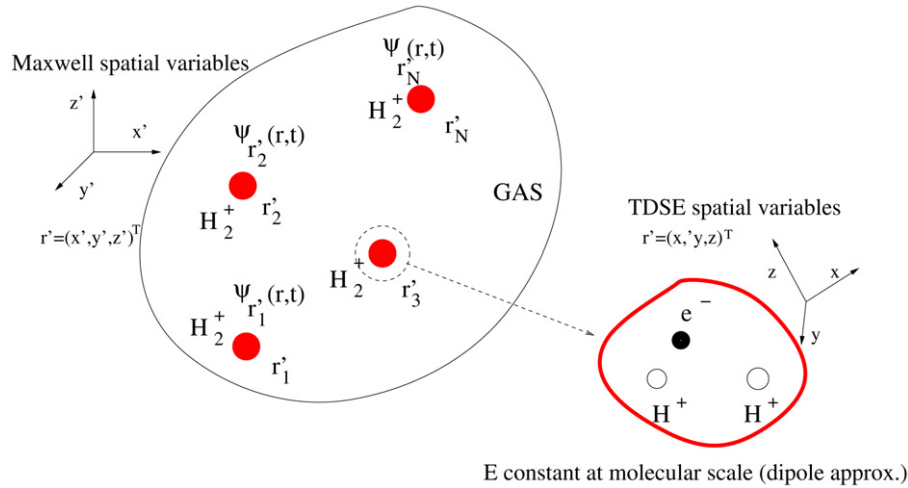


Fig. 6. Configuration.

we get a new formulation of the TDSE [4,18]:

$$i \partial_t \psi_{\mathbf{r}'}(\mathbf{r}, R, t) = \left[-\frac{1}{2} \Delta_{\mathbf{r}} + V_c(\mathbf{r}, R) + \mathbf{r} \cdot \mathbf{E}_{\mathbf{r}'}(t) + V_i(R) - \frac{1}{m_p} \Delta_R \right] \psi_{\mathbf{r}'}(\mathbf{r}, R, t), \quad (5)$$

with $c\mathbf{E}_{\mathbf{r}'} = -\partial\mathbf{A}_{\mathbf{r}'}/\partial t$ denoting the electric field. In this paper, the numerical computations will be done in the length gauge.

Ideally the electric field dynamics modeling would be given by the microscopic Maxwell's equations coupled with the TDSE's and will be done in a future work. A full description of the microscopic Maxwell's equations can be found in [23]. A close approach is proposed in [24], where the authors study the microscopic Maxwell's equations but coupled with classical dynamics equations to describe the particle motions. We will here consider the macroscopic Maxwell's equations that correspond to a spatial average of the microscopic ones. These equations are typically valid in a domain equal or exceeding a size of 10^{-18} cm^3 with a sufficiently high molecular density (see again [23]). The macroscopic 3-D-Maxwell's equations written in atomic units, are:

$$\begin{cases} \partial_t \mathbf{B}(\mathbf{r}', t) = -c \nabla_{\mathbf{r}'} \times \mathbf{E}(\mathbf{r}', t), \\ \partial_t \mathbf{E}(\mathbf{r}', t) = c \nabla_{\mathbf{r}'} \times \mathbf{B}(\mathbf{r}', t) - 4\pi \partial_t \mathbf{P}(\mathbf{r}', t), \\ \nabla_{\mathbf{r}'} \cdot (\mathbf{E}(\mathbf{r}', t) + 4\pi \mathbf{P}(\mathbf{r}', t)) = 0, \\ \nabla_{\mathbf{r}'} \cdot \mathbf{B}(\mathbf{r}', t) = 0. \end{cases} \quad (6)$$

Under the dipole approximation the polarization \mathbf{P} for a molecule located at \mathbf{r}' is given by:

$$\mathbf{P}(\mathbf{r}', t) = -n(\mathbf{r}') \int \psi_{\mathbf{r}'}(\mathbf{r}, R, t) \cdot \mathbf{r} \cdot \psi_{\mathbf{r}'}^*(\mathbf{r}, R, t) dR d\mathbf{r}, \quad (7)$$

where $n(\mathbf{r}')$ denotes the molecular density defined below. The sign comes from the electron charge. The polarization \mathbf{P} ensures then the coupling between the Schrödinger and Maxwell's equations (see Fig. 6). In this model we suppose that for a molecule localized in \mathbf{r}' the polarization $\mathbf{P}(\mathbf{r}', t)$ is constant in an *elementary volume of gas* around \mathbf{r}' . This volume $v_e(\mathbf{r}')$ has to be chosen large enough such that the macroscopic Maxwell's equations remain valid (at least 10^{-18} cm^3) and small enough to capture high order transmitted electric field frequencies. In each elementary volume of gas v_e , the electric field and the polarization are constant and we have to solve one unique TDSE. However v_e contents $n(\mathbf{r}') \times v_e(\mathbf{r}')$ molecules. The choice of the elementary volume of gas will be discussed in detail in the numerical approach section.

The model is then given by Eqs. (5)–(7).

Note that another approach consists in computing directly the dipolar acceleration:

$$\mathbf{d}(\mathbf{r}', t) = \partial_{tt}^2 \mathbf{P}(\mathbf{r}', t) = -n(\mathbf{r}') \int \psi_{\mathbf{r}'}(\mathbf{r}, R, t) (\nabla_{\mathbf{r}} V_c(\mathbf{r}, R) + \mathbf{E}(t)) \psi_{\mathbf{r}'}^*(\mathbf{r}, R, t) dR d\mathbf{r}, \quad (8)$$

Now, let us denote by Ω_M the Maxwell domain. The molecules are located in a subdomain $\Omega_m \subset \Omega_M$, and the vacuum regions are denoted by Ω_0 such that: $\Omega_M = \Omega_m \cup \Omega_0$ (see Figs. 7, 8 for 1-D configuration). Initially the laser-pulse of frequency ω and intensity I is defined as:

$$\begin{cases} \mathbf{E}(\mathbf{r}', 0) = \mathbf{E}_0(\mathbf{r}') f_\omega(\mathbf{r}'), & \mathbf{r}' \in \Omega_0, \\ \mathbf{E}(\mathbf{r}', 0) = 0, & \text{elsewhere.} \end{cases}$$

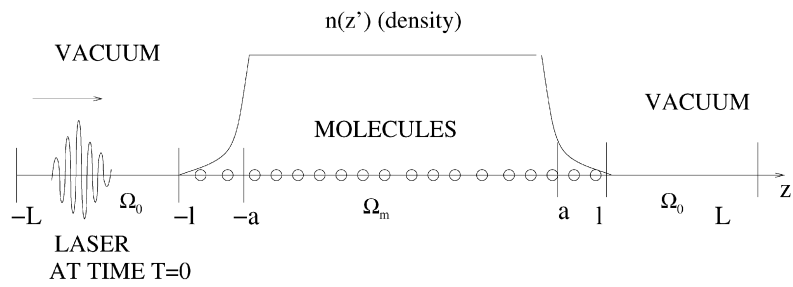


Fig. 7. Physical configuration: 1-D-cut (1).

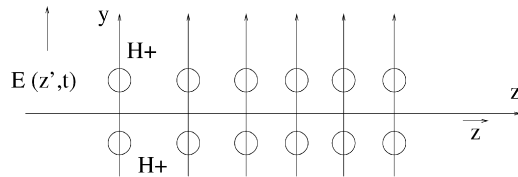


Fig. 8. Physical configuration: 1-D-cut (2).

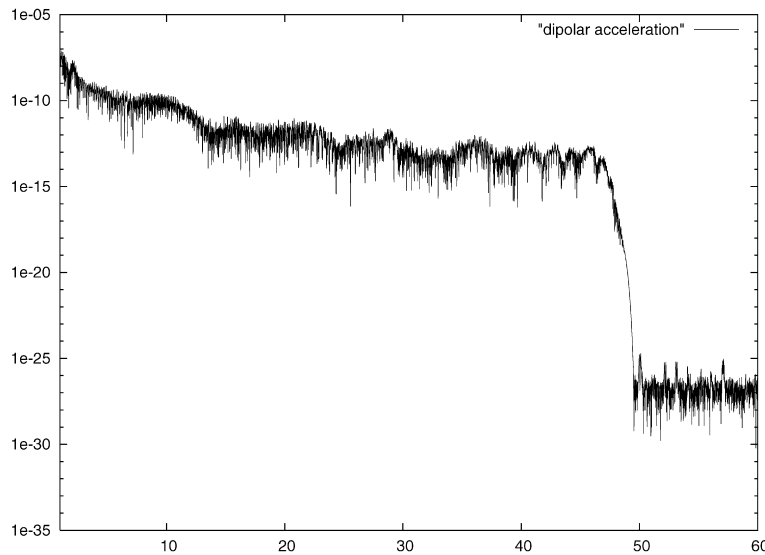


Fig. 9. $|\hat{E}(\omega)|^2$, for a single molecule, and a few-cycle laser pulse at $I = 10^{14}$ W/cm² and $\lambda = 800$ nm ($\omega_0 = 0.057$). In abscissa: harmonic order N , with $\omega = N\omega_0$ and ω_0 the incident electric field frequency.

The function f is usually sinusoidal, and E_0 is a Gaussian function $\mathbf{E}_0(\mathbf{r}') = I e^{-c_x(x'-x_c)^2 - c_y(y'-y_c)^2 - c_z(z'-z_c)^2} \mathbf{e}_{y'}$ even if for usual cases the beam is sufficiently large so that along the propagation axis, we can again neglect x' and y' dependences. Quantities c_x, c_y, c_z , depend on the pulse shape.

The harmonic spectrum of the transmitted field, denoted by \mathbf{E}_T , possesses in theory [25], a frequency cut-off denoted by ω_c (see Fig. 9) where $\omega_c = I_p + 3.17U_p = N\omega$ for recollision of the electron with the parent ion [14,19]. I_p is the ionization potential, and $U_p = I/4\omega^2$ (a.u.) for intensity I and frequency ω . N is the harmonic order at the cut-off frequency. Collisions with neighboring ions such as in molecules produce larger orders N , due to large collision energies exceeding $3.17U_p$ [8]. It is then possible but *not done here*, to filter this transmitted field, around ω_c and to pick-up an “intense” pulse denoted by E_F with a very high frequency:

$$\mathbf{E}_F(t) = \frac{1}{2\pi} \int_{\omega_c - \Delta\omega}^{\omega_c + \Delta\omega} \hat{\mathbf{E}}_T(\omega) e^{i\omega t} d\omega.$$

In Fig. 9 for instance, the frequency cut is approximately 50 times larger than the incident laser one. The duration Δt of such a pulse follows the relation $\Delta t \cdot \Delta\omega \sim 1$. See, for instance, [7,37] or [11] for control aspects. Note that, this problem constitutes typically a multiscale physical problem as the TDSE characteristic lengths and times are much smaller than the Maxwell’s equation characteristic ones.

There exist many other models describing the physical phenomena presented above. The most common ones are the *nonlinear Maxwell models* (NLME), and consist in calculating the polarization as a perturbative expansion of the susceptibility (linear, quadratic, cubic, and so on):

$$\mathbf{P}(\mathbf{r}', t) = \chi^{(1)} \cdot \mathbf{E} + \chi^{(2)} \cdot \mathbf{E}^2 + \chi^{(3)} \cdot \mathbf{E}^3 + \dots + \chi^{(\sigma)} \cdot \mathbf{E}^\sigma,$$

instead of deducing it from the molecular wavefunctions. These models allow for example to simulate the behavior of low intensity lasers with low harmonic generation. Under slowly varying envelope approximation it is also possible to derive the *nonlinear Schrödinger models* (NLSE). As our transmitted fields possess high order harmonics these models are not applicable here due to the high nonlinear regime. Indeed in these models only first order nonlinearities are taken into account (usually $\sigma \leq 5$). Moreover the ionization is not considered in these models (see Figs. 3, 4).

The Maxwell–Bloch equations constitutes a more precise model where the polarization \mathbf{P} is obtained from the TDSE *via* the Bloch equation coupled with the Maxwell’s equations. More precisely, supposing the nuclei fixed, the TDSE can be written in a compact form:

$$i \partial_t \psi = [H_0 + L(\mathbf{E})] \psi,$$

where H_0 is the free Hamiltonian (without laser) and $L(\mathbf{E})$ denotes the laser operator and \mathbf{E} the electric field. We then compute the N first eigenvalues and associated eigenvectors of the field free Hamiltonian operator (energy levels $(\omega_j)_j$ and associated eigenfunctions, $(\phi_j)_j$), that is, supposing no degeneracy:

$$H_0 \phi_j = \phi_j \omega_j, \quad \forall j \in \{1, \dots, N\}.$$

We can then deduce the so-called dipolar matrix $\boldsymbol{\mu} \in M_N(\mathbb{C}^3)$ obtained using the position operator and the eigenfunctions of the field free Hamiltonian. Then we have to solve a set of differential equations on the electronic density matrix $\boldsymbol{\rho} = (\rho_{jk})_{jk} \in M_N(\mathbb{C})$:

$$\begin{cases} \partial_t \rho_{jk} = -i(\omega_j - \omega_k) \rho_{jk} - \frac{2i\pi}{h} [\mathbf{V}, \boldsymbol{\rho}], & (j, k) \in \{1, \dots, N\}^2, \\ \boldsymbol{\rho}(\cdot, t=0) = (\int \phi_j \phi_k^*)_{jk} \end{cases}$$

with $\mathbf{V} = -\boldsymbol{\mu} \cdot \mathbf{E}$ under the dipole approximation, and where $[\cdot, \cdot]$ is the Lie bracket. Finally denoting by \mathcal{N} the molecular density, the polarization is given by: $\mathbf{P} = \mathcal{N} \text{tr}(\boldsymbol{\mu} \cdot \boldsymbol{\rho})$. A detailed numerical study of this model can be found in [12] and [35]. To understand the validity of this model, let us emphasize that the polarization \mathbf{P} is obtained from the energy levels of the field free Hamiltonian. As is well known the computation of the eigenelements of the Hamiltonian operator is numerically very costly, so that N is in practice limited to very small numbers (less than 5 usually). With such a limited model it is then *a priori* not possible to reach the continuous part of the Hamiltonian (ionization) then to compute high order harmonics with very intense laser pulses (typically of the order of the Coulomb potential field intensity).

2.2. Existence and regularity for the TDSE

In this section we are interested in the existence and regularity of solutions for the TDSE (5). To do this, we will use the Fourier transform set of the Sobolev space H^1 :

$$H_1 = \left\{ u \in L^2(\mathbb{R}^4), \int_{\mathbb{R}^4} (1 + \|\mathbf{r}, R\|^2) |u(\mathbf{r}, R)|^2 \mathbf{d}\mathbf{r} \mathbf{d}R < \infty \right\}.$$

From Baudouin and Puel [9,10], we can easily deduce that for $\mathcal{L} \in L^\infty(0, T; C_b^2(\mathbb{R}^4))$ and if $u_0 \in H^1 \cap H_1$, then there exists a unique solution u in $C^0(0, T; H^1 \cap H_1)$ such that

$$\left(i \partial_t + \frac{\Delta_{\mathbf{r}}}{2} + \frac{\Delta_R}{m_p} + \mathcal{L}(\mathbf{r}, R, t) \right) u(\mathbf{r}, R, t) = 0, \quad u(\mathbf{r}, R, 0) = u_0(\mathbf{r}, R).$$

Furthermore, for $K > 0$ such that

$$\|V\|_{L^\infty(0, T; C_b^2(\mathbb{R}^4))} \leq K$$

then there exists $C_{T, K}$ such that

$$\|u\|_{C^0(0, T; H^1 \cap H_1)} \leq C_{T, K} \|u_0\|_{H^1 \cap H_1}.$$

Considering now (5), let us suppose that for all $T > 0$, $\mathbf{E} \in L^\infty(0, T)$ and $\partial_t \mathbf{E} \in L^1(0, T)$. The laser field $\mathbf{r} \cdot \mathbf{E}(t)$ we consider is not *a priori* nonzero for all $\mathbf{r} \in \mathbb{R}^3$. Physically it is obviously not true, so that we will consider a function χ defined as follows: $\chi : (\mathbf{r}, R) \mapsto \chi(\mathbf{r}, R)$ in $C_b^2(\mathbb{R}^4)$ and $\chi(\mathbf{r}, R) = \mathbf{r}$ on a compact set Ω_1 of \mathbb{R}^4 and $\chi(\mathbf{r}, R)$ is zero outside a set Ω_2 containing strictly Ω_1 . Such a function can easily be constructed by convolution of \mathbf{r} and a plateau function. Then we can prove:

Theorem 2.1. *Let us consider the following TDSE:*

$$i \partial_t \psi(\mathbf{r}, R, t) = \left[-\frac{1}{2} \Delta_{\mathbf{r}} + V_c(\mathbf{r}, R) - \frac{1}{m_p} \Delta_R + V_i(R) - \chi(\mathbf{r}, R) \cdot \mathbf{E}(t) \right] \psi(\mathbf{r}, R, t).$$

$\forall T > 0$, suppose that $\mathbf{E} \in L^\infty(0, T)$ and $\partial_t \mathbf{E} \in L^1(0, T)$. Then there exists $C_T > 0$ such that, for all $\psi_0 \in H^1 \cap H_1$, there exists a solution unique $\psi \in L^\infty(0, T; H^1 \cap H_1)$ and

$$\|\psi(t)\|_{L^\infty(0, T; H^1 \cap H_1)} \leq C_T \|\psi_0\|_{H^1 \cap H_1}.$$

The proof is based an energy estimate in $H_1 \cap H^1$ via a Gronwall inequality and a compactness argument to extract a convergent subsequence. As it can be derived with some elementary modifications from the proof of Theorem 2.1 in [10] and is very close of existing results, for instance, [22], we present it in Appendix A.

We can in fact improve the previous results. Under regularity assumptions on the electric field we could prove (using again [9]) that for $u_0 \in H^2 \cap H_2$ the existence of a unique solution in $L^\infty(0, T; H^2 \cap H_2)$.

These results ensure us that the regularity in space of the initial data will be conserved in time. This is a crucial point in the choice of the numerical scheme for the TDSE. Indeed as no singularity will appear in time, even a simple finite difference approach can be accurate enough.

The existence of solutions for the coupled system Maxwell–Schrödinger has yet to be proved; in particular the regularity of the polarization (linking the two systems) is useful in our numerical approach. We can expect that the polarization regularity on \mathbf{r}' comes from the incoming electric field spatial regularity. Some interesting results about this coupling can be found, for instance, in [21], where the existence of global smooth and weak Maxwell–Bloch solutions is presented.

3. Numerical approach

We describe in this section our numerical method to approximate the Maxwell–Schrödinger system presented above. We will focus on the polarization computation that allows the coupling between the Maxwell’s equations and TDSE’s. The numerical approach proposed here is relatively standard (excepted for the TDSE boundary conditions, but discussed in [27] and in details in [26]). In fact as no specific shape for the physical domains is imposed and as no regularity degeneracy will occur, simple finite difference methods can be used to approximate our equations. Note however, that the use of spectral could also be of interest. *Let us recall that the goal of this work is to validate the model using as much as possible effective numerical methods, but at this point it is not to develop the most performing ones.*

Suppose to simplify the notations that the Maxwell computational domain is given by the following set $\Omega_M = [-L_x, L_x] \times [-L_y, L_y] \times [-L_z, L_z]$, $L_x, L_y, L_z > 0$ and the molecules are located in $\Omega_m = [-\ell_x, \ell_x] \times [-\ell_y, \ell_y] \times [-\ell_z, \ell_z] \subset \Omega_M$, and the vacuum region is $\Omega_0 = [-L_x, L_x] \times [-L_y, L_y] \times [-L_z, L_z] / [-\ell_x, \ell_x] \times [-\ell_y, \ell_y] \times [-\ell_z, \ell_z]$ with $\ell_x < L_x$, $\ell_y < L_y$ and $\ell_z < L_z$. In this framework, introducing some positive constants $0 < a < \ell < L$, the molecular density can be given by:

$$n(\mathbf{r}') = \begin{cases} 0 & \text{if } \ell < \|\mathbf{r}'\| < L, \\ n_0 \exp(-(\|\mathbf{r}'\| - a)^2) & \text{if } a < \|\mathbf{r}'\| < \ell, \\ n_0 & \text{if } \|\mathbf{r}'\| \leq a, \end{cases}$$

where $n_0 \in \mathbb{R}_+^*$ (mol/cm³). Such a density choice will allow us in particular to numerically reduce the reflections of the incoming electric field on the “boundaries” of the gas. The TDSE is approximated by a finite difference Crank–Nicolson scheme in time, and the Laplace operator is approximated using a 3-points stencil. Such a second order scheme, allows to preserve the ℓ^2 -norm. The Yee scheme is used to solve the Maxwell’s equations [40]. It consists in a predictor–corrector finite difference scheme where the electric and magnetic fields are computed on two spatial and temporal staggered grids. Under a CFL condition this is a stable and order two scheme. At this point it is important to recall that to be valid the macroscopic Maxwell’s equations have to be applied on a sufficiently large domain (as it is obtained by a spatial average on microscopic Maxwell’s equations). If we denote by $\Delta \mathbf{r}'_M$ the Maxwell space step, we should have: $\|\Delta \mathbf{r}'_M\| \times n(\mathbf{r}') \gg 1$ but also have $\|\Delta \mathbf{r}'_M\| < \lambda_{\min}/C$, with λ_{\min} corresponding to the highest harmonic created during the HHG process and where C is a positive constant at least larger than 5. In each Maxwell cell, a large number of molecules is then contained ($n(\mathbf{r}') \times \Delta \mathbf{r}'_M$), but in practice we solve only one TDSE to determine the local polarization \mathbf{P} . Then $\Delta \mathbf{r}'_M$ corresponds to the elementary volume of gas v_e , introduced in the previous section. The simulation has then multiple scales as $\|\Delta \mathbf{r}'_M\| \gg \|\Delta \mathbf{r}_S\|$ (see Fig. 10). And obviously $\Delta t_M \gg \Delta t_S$ where Δt_S , Δt_M are, respectively, the Schrödinger and Maxwell solver time steps. We then set

$$\bar{N} = E \left[\frac{\Delta t_M}{\Delta t_S} \right].$$

Now denoting by \mathcal{S}_h the discrete Schrödinger operator and by \mathcal{B}_h the discrete Maxwell operator, the global coupled numerical scheme is written as the following splitting scheme (here written at order 1, but is computed at order 2 (Strang splitting) to preserve

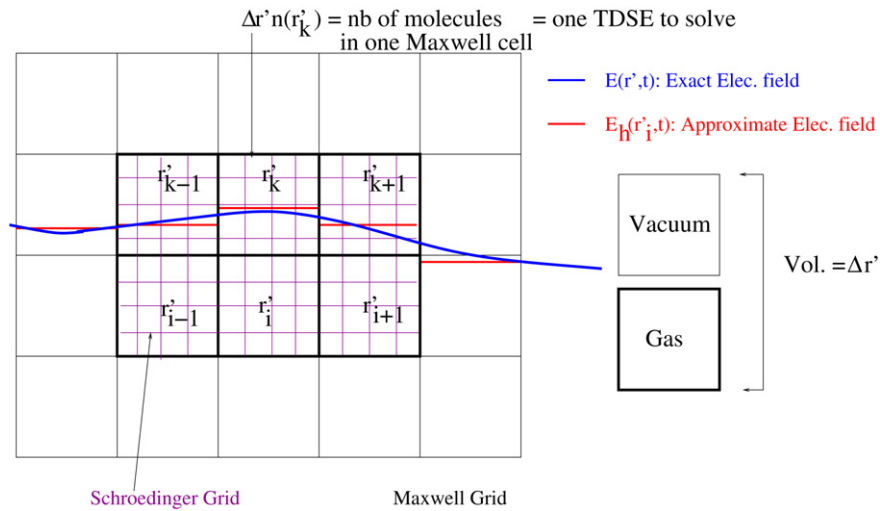


Fig. 10. Maxwell and Schrödinger grids.

the Maxwell and Schrödinger solvers order), from time t^n to time t^{n+1} :

$$\begin{cases} \mathbf{E}^{n+1} \leftarrow e^{\Delta t_M \mathcal{B}_h^n} \mathbf{E}^n, & \forall \mathbf{r}' \in \Omega_M, & \text{solving the Maxwell's equations,} \\ \psi^{n+1} \leftarrow e^{[\Delta t_M - (\bar{N}-1)\Delta t_S] \mathcal{S}_h^n} e^{(\bar{N}-1)\Delta t_S \mathcal{S}_h^n} \psi^n, & & \text{solving the TDSE's in each "Maxwell cell",} \\ \mathbf{P}^{n+1} \leftarrow \psi^{n+1}, & & \text{by definition of the polarization.} \end{cases}$$

3.1. Numerical schemes

Fig. 10 summarizes the numerical configuration.

3.1.1. Time-dependent Schrödinger equation

Let us consider the TDSE beyond the Born–Oppenheimer approximation:

$$i \partial_t \psi_{\mathbf{r}'}(\mathbf{r}, R, t) = (A + B + C_{\mathbf{r}'}) \psi_{\mathbf{r}'}(\mathbf{r}, R, t)$$

with

$$A = -\frac{1}{2} \Delta_{\mathbf{r}} + V_c, \quad B = -\frac{1}{m_p} \Delta_R + V_i, \quad C_{\mathbf{r}'} = \mathbf{r} \cdot \mathbf{E}_{\mathbf{r}'}(t).$$

The domain we work on is then given by $\Omega_S \times]0, R_\infty]$, with R_∞ the largest numerical inter-nuclear distance. The space steps are given by $\Delta \mathbf{r}_S = (\Delta x_S, \Delta y_S, \Delta z_S)^T$ and ΔR , and in the following Δt_S will denote the time step of the numerical scheme approximating the TDSE.

The first step consists in computing the initial data of the TDSE obtained from the smallest eigenvalue and associated eigenvector of the field free Hamiltonian $A + B$. It corresponds to the initial bound energy state. This is done here using a classical procedure (Arnoldi solver), see Fig. 11.

Setting ψ^n an approximation of $\psi(\cdot, \cdot, t^n)$, the modified Crank–Nicolson scheme we consider, is:

$$\begin{cases} i \frac{\psi^{n+1/2} - \psi^n}{\Delta t_S} = -\frac{\Delta_{\mathbf{r}} \psi^{n+1/2}}{4} + \frac{V_c}{2} \psi^{n+1/2} - \frac{\Delta_{\mathbf{r}} \psi^n}{4} + \left(\frac{V_c}{2} + \mathbf{r} \cdot \mathbf{E}^n \right) \psi^n, \\ i \frac{\psi^{n+1} - \psi^{n+1/2}}{\Delta t_S} = -\frac{\Delta_R \psi^{n+1}}{2m_p} + \frac{V_i}{2} \psi^{n+1} - \frac{\Delta_R \psi^{n+1/2}}{2m_p} + \frac{V_i}{2} \psi^{n+1/2}. \end{cases} \quad (9)$$

This approach is classical and allows in particular to preserve, when the electric field is zero, the ℓ^2 -norm of ψ and is of order 2. Numerically, the computation of the sparse linear system coming from the semi-implicit Crank–Nicolson scheme is given by a LU-preconditioned GMRES iterative method (see [34]). The storage is a compressed row storage (C.R.S.).

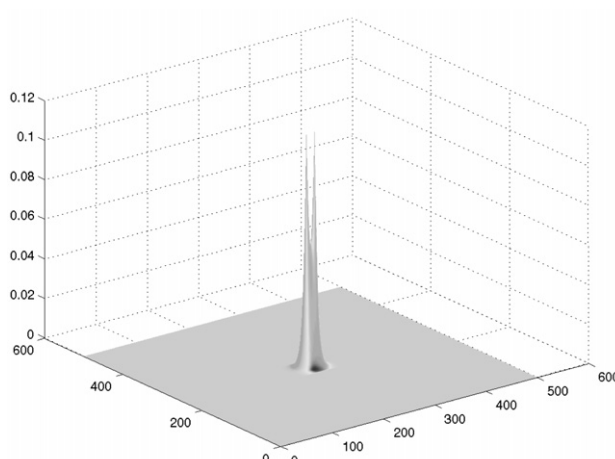


Fig. 11. Initial data in arbitrary units: probability $|\psi(x, y, z, t = 0)|^2$ at $R = R_0 = 2$ a.u.

3.1.2. Maxwell's equations

The Maxwell's equations are approximated using the Yee scheme [40] with Mur's absorbing boundary conditions [31]. This is a stable order 2 scheme under a CFL condition:

$$\Delta t_M \leq 1/c \sqrt{\frac{1}{\Delta x_M'^2} + \frac{1}{\Delta y_M'^2} + \frac{1}{\Delta z_M'^2}}. \quad (10)$$

In vacuum we then use the classical Yee scheme and we add the polarization derivative in time $\partial_t \mathbf{P}$, when the laser interacts with the gas. As discussed above the space step choice is crucial (see Fig. 10). An important issue is to guarantee that inside the gas the divergence condition on $\mathbf{D} = \mathbf{E} + 4\pi \mathbf{P}$, $\nabla \cdot \mathbf{D} = 0$ (Maxwell–Gauss equation) is verified at the discrete level.

Proposition 3.1. *The condition¹ $\nabla_h \cdot \mathbf{D}_h^n = 0$ is numerically verified by the modified Yee scheme for all $n \in \mathbb{N}$, provided that $\nabla_h \cdot \mathbf{D}_h^0 = 0$.*

Proof. It is well known that the Yee scheme in vacuum leads to

$$\nabla_h \cdot \mathbf{E}_h^{n+1} = \nabla_h \cdot \mathbf{E}_h^n.$$

This allows to prove in vacuum, that the Yee scheme verifies $\nabla_h \mathbf{E}_h^n = 0$ for all $n \in \mathbb{N}$, provided that $\nabla_h \mathbf{E}_h^0 = 0$. In the non-homogeneous case, the same calculations lead us to the following discrete equation:

$$\nabla_h \cdot \mathbf{E}_h^{n+1} + 4\pi \Delta t_M \nabla_h (\partial_t \mathbf{P}_h^{n+1}) = \nabla_h \cdot \mathbf{E}_h^n.$$

That is, supposing \mathbf{P} regular enough in time and space (see next section):

$$\nabla_h \cdot \mathbf{E}_h^{n+1} + 4\pi \Delta t_M \partial_t (\nabla_h \mathbf{P}_h^{n+1}) = \nabla_h \cdot \mathbf{E}_h^n.$$

Now using the approximation of the partial derivative in time, we have:

$$\partial_t (\nabla_h \mathbf{P}_h^{n+1}) = \frac{\nabla_h \mathbf{P}_h^{n+1} - \nabla_h \mathbf{P}_h^n}{\Delta t_M},$$

then

$$\nabla_h \cdot \mathbf{E}_h^{n+1} + 4\pi \Delta t_M \left(\frac{\nabla_h \mathbf{P}_h^{n+1} - \nabla_h \mathbf{P}_h^n}{\Delta t_M} \right) = \nabla_h \cdot \mathbf{E}_h^n.$$

So that:

$$\nabla_h \cdot \mathbf{E}_h^{n+1} + 4\pi \nabla_h \mathbf{P}_h^{n+1} = \nabla_h \cdot \mathbf{E}_h^n + 4\pi \nabla_h \mathbf{P}_h^n.$$

Then by simple induction, we deduce that provided that $\nabla_h \cdot \mathbf{D}_h^0 = 0$, $\nabla_h \cdot \mathbf{D}_h^n = 0$ for all n . \square

¹ $\mathbf{E}_h, \mathbf{D}_h, \nabla_h$ denote the discrete approximations of \mathbf{E}, \mathbf{D} and ∇ .

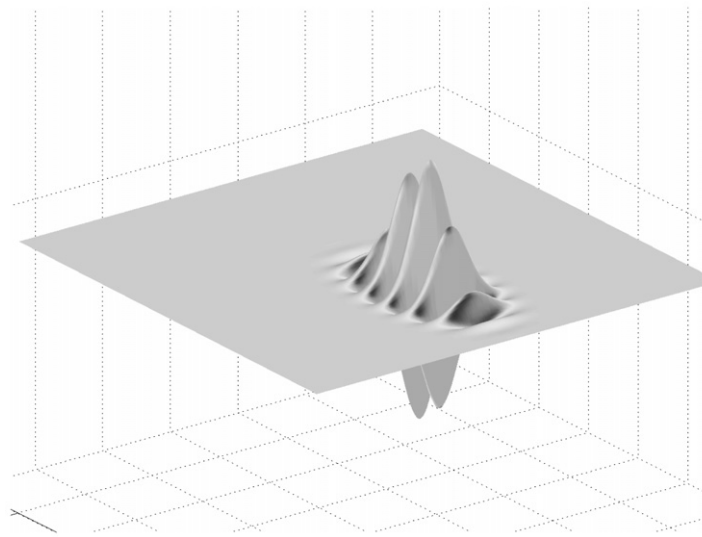


Fig. 12. Initial electric field $E(x', y', z' = z_0, t = 0)$ — x', y' -plan (z' is fixed)— $\lambda \sim 800$ nm and ~ 6 cycles.

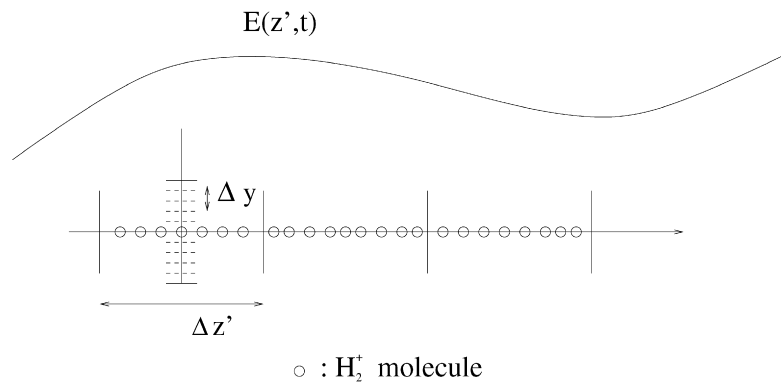


Fig. 13. Maxwell and Schrödinger scales (1-D).

This result guarantees us the charge conservation (Eqs. (1) and (3) in (6)). The typical initial data we consider are as Fig. 12. And finally we have:

Theorem 3.1. *The global scheme approximating the Maxwell–Schrödinger model, is an order 2 scheme, stable under the CFL condition (10).*

Proof. It is sufficient to notice that the TDSE's and Maxwell's equations are solved using order 2 numerical schemes, and are coupled together with an order 2 Strang splitting. \square

3.2. Polarization computation

The polarization computation is central in this work as it allows to couple the Maxwell's equations and TDSE's. As said above the polarization is deduced from the TDSE by (7). In practice in each Maxwell-cell we solve numerically one single TDSE and we deduce the local polarization for a physical volume of size $\Delta x'_M \times \Delta y'_M \times \Delta z'_M$ and containing $n(\mathbf{r}') \Delta x'_M \times \Delta y'_M \times \Delta z'_M$ molecules.

Remark 1. For a one-dimensional gas propagation of 100 cycles laser pulse of wavelength 800 nm interacting with molecules, we would have to solve numerically at each iteration 8000 (80×100) TDSE's, if the Maxwell cell size is equal to $\Delta z'_M = 10$ nm (one TDSE per Maxwell cell). As noticed above, the non-Born–Oppenheimer TDSE we have to solve is 4D, and is then costly in CPU time. We then propose a technique based on a simple Taylor expansion that allows us to reduce the numerical complexity, supposing the polarization smooth in space. As discussed above, this assumption seems *a priori* valid when the electric field is smooth enough and its wavelength encompasses a large number of molecules (see Fig. 13).

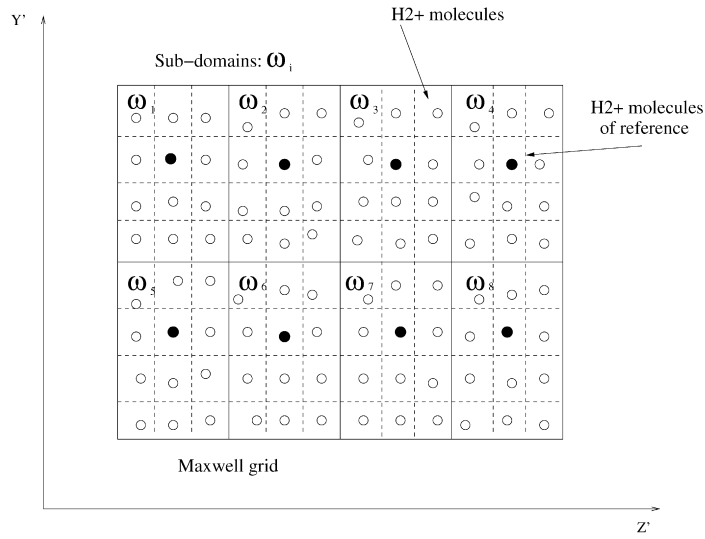


Fig. 14. Decomposition of the domain.

3.3. Decreasing the polarization computation cost

We propose in this section a way to reduce the computation cost of the polarization in a gas. The principle is based on an interpolation using a Taylor expansion and the dipole approximation. We first make a partition of the domain $\Omega_M = \bigcup_{i=1, \dots, I-1} [\omega'_i, \omega'_{i+1}[$ where I is a small integer. We suppose that each subdomain ω_i contains a sufficiently large number of Maxwell cells. For each subdomain ω_i , we choose a reference cell $\mathbf{r}'_{i,0}$ (localized, for example, in the “center” of the subdomain, see Fig. 14). For this cell we compute the corresponding TDSE, that is:

$$i \partial_t \psi_{\mathbf{r}'_{i,0}}(\mathbf{r}, R, t) = \left(-\frac{1}{2} \Delta_{\mathbf{r}} + V_c(\mathbf{r}, R) - \frac{1}{m_p} \Delta_R + V_i(R) + \mathbf{r} \cdot \mathbf{E}_{\mathbf{r}'_{i,0}}(t) \right) \psi_{\mathbf{r}'_{i,0}}(\mathbf{r}, R, t).$$

and the corresponding polarization constant in the associated Maxwell cell is:

$$\mathbf{P}(\mathbf{r}'_{i,0}, t) = -n(\mathbf{r}'_{i,0}) \int \psi_{\mathbf{r}'_{i,0}}(\mathbf{r}, R, t) \cdot \mathbf{r} \cdot \psi_{\mathbf{r}'_{i,0}}^*(\mathbf{r}, R, t) \, d\mathbf{r} \, dR. \quad (11)$$

For every other cell located in $\mathbf{r}'_j \in \omega_i$ we have by Taylor expansion:

$$\mathbf{P}(\mathbf{r}'_j, t) = \mathbf{P}(\mathbf{r}'_{i,0}, t) + \nabla_{\mathbf{r}'} \mathbf{P}(\mathbf{r}'_{i,0}, t) \cdot (\mathbf{r}'_j - \mathbf{r}'_{i,0}) + \mathcal{O}(\|\mathbf{r}'_j - \mathbf{r}'_{i,0}\|^2). \quad (12)$$

Then we deduce the value of the polarization for every cell of the subdomain ω_i . In this goal, it is necessary to compute $\nabla_{\mathbf{r}'} \mathbf{P}(\mathbf{r}'_{i,0}, t)$: by derivation in \mathbf{r}' of (11), we obtain

$$\begin{aligned} \nabla_{\mathbf{r}'} \mathbf{P}(\mathbf{r}'_{i,0}, t) &= -n(\mathbf{r}'_{i,0}) \int \nabla_{\mathbf{r}'} \psi_{\mathbf{r}'_{i,0}}(\mathbf{r}, R, t) \cdot \mathbf{r} \cdot \psi_{\mathbf{r}'_{i,0}}^*(\mathbf{r}, R, t) \, d\mathbf{r} \, dR \\ &\quad - n(\mathbf{r}'_{i,0}) \int \psi_{\mathbf{r}'_{i,0}}(\mathbf{r}, R, t) \cdot \mathbf{r} \cdot \nabla_{\mathbf{r}'} \psi_{\mathbf{r}'_{i,0}}^*(\mathbf{r}, R, t) \, d\mathbf{r} \, dR \\ &\quad - (\nabla_{\mathbf{r}'} n)(\mathbf{r}'_{i,0}) \int \psi_{\mathbf{r}'_{i,0}}(\mathbf{r}, R, t) \cdot \mathbf{r} \cdot \psi_{\mathbf{r}'_{i,0}}^*(\mathbf{r}, R, t) \, d\mathbf{r} \, dR. \end{aligned}$$

Then to obtain $\nabla_{\mathbf{r}'} \mathbf{P}(\mathbf{r}'_{i,0}, t)$ we compute $\nabla_{\mathbf{r}'} \psi_{\mathbf{r}'_{i,0}}(\mathbf{r}, R, t)$ solving the following system, obtained by derivation in \mathbf{r}' of the TDSE,

$$\begin{aligned} i \partial_t (\nabla_{\mathbf{r}'} \psi_{\mathbf{r}'_{i,0}}(\mathbf{r}, R, t)) &= \left(-\frac{1}{2} \Delta_{\mathbf{r}} + V_c(\mathbf{r}, R) - \frac{1}{m_p} \Delta_R + V_i(R) + \mathbf{r} \cdot \mathbf{E}_{\mathbf{r}'_{i,0}}(t) \right) \nabla_{\mathbf{r}'} \psi_{\mathbf{r}'_{i,0}}(\mathbf{r}, R, t) \\ &\quad + i (\nabla_{\mathbf{r}'} \mathbf{E}_{\mathbf{r}'_{i,0}}(t)) \cdot \mathbf{r} \cdot \psi_{\mathbf{r}'_{i,0}}(\mathbf{r}, R, t). \end{aligned} \quad (13)$$

The numerical scheme to solve the previous system, is simply deduced from our modified Crank–Nicolson scheme:

$$(\nabla_{\mathbf{r}'} \psi_{\mathbf{r}'_{i,0}})^{n+1} = \frac{(\nabla_{\mathbf{r}'} \psi_{\mathbf{r}'_{i,0}})^{n+1}}{2} + \frac{(\nabla_{\mathbf{r}'} \psi_{\mathbf{r}'_{i,0}})^n}{2} - \frac{i}{2} \mathcal{H}_{\mathbf{r}'_{i,0}}^{n+1} (\nabla_{\mathbf{r}'} \psi_{\mathbf{r}'_{i,0}})^{n+1} - \frac{i}{2} \mathcal{H}_{\mathbf{r}'_{i,0}}^n \nabla_{\mathbf{r}'} \psi_{\mathbf{r}'_{i,0}}^n + i (\nabla_{\mathbf{r}'} \mathbf{E}_{\mathbf{r}'_{i,0}})^{n+1} \cdot \mathbf{r} \cdot \psi_{\mathbf{r}'_{i,0}}^{n+1}. \quad (14)$$

In (14) the quantity $\psi_{\mathbf{r}'_{i,0}}^{n+1}$ is supposed to have been previously computed by the numerical scheme for the TDSE with $\mathcal{H}_{i,0}^n$ given by:

$$\mathcal{H}_{i,0}^n = \left(-\frac{1}{2}\Delta_{\mathbf{r}} + V_c(\mathbf{r}, R) - \frac{1}{m_p}\Delta_R + V_i(R) + \mathbf{r} \cdot \mathbf{E}_{\mathbf{r}'_{i,0}}^n \right) (1, 1, 1)^T, \quad n > 0.$$

Finally, for each subdomain ω_i we compute $\psi_{\mathbf{r}'_{i,0}}(\mathbf{r}, R, t)$ and $\nabla_{\mathbf{r}'}\psi_{\mathbf{r}'_{i,0}}(\mathbf{r}, R, t)$ to deduce linearly from $\mathbf{P}(\mathbf{r}'_{i,0}, t)$ the polarization for each cell located in \mathbf{r}'_j of this subdomain. The error due to this process is naturally here at order one. It is possible to increase the order using a higher order Taylor expansion. In this case, it would be necessary to compute $\nabla_{\mathbf{r}'}^2\psi_{\mathbf{r}'_{i,0}}(\mathbf{r}, R, t)$ obtained by double derivation in \mathbf{r}' of the TDSE. We can then deduce easily the following result:

Proposition 3.2. *Supposing the polarization and the molecular density smooth enough, the approximation proposed above in each \mathbf{r}'_j of a subdomain ω_i , is of order 1 or 2 depending on the Taylor expansion order.*

In practice we can expect in some cases, a strong reduction of the number of TDSE's to solve. The subdomains size will again depend on the highest transmitted electric field harmonics, then on the intensity and frequency of the incoming laser pulses. The higher the harmonics will be, the smaller the size of the subdomains will be chosen. Indeed, if the laser is intense and ultrashort, the cut-off frequency will be large, so that to capture high frequencies (until cut-off frequency) the grid (and the subdomains) has to be fine enough.

Taking into account the previous method to reduce the computational cost of the polarization, that is the number of TDSE's to solve, we have the following temporal scheme from t^n to t^{n+1} , denoting by $I - 1$ the number of subdomains, with $I \ll$ number of cells in the Maxwell grid:

$$\left\{ \begin{array}{ll} \mathbf{E}^{n+1} \leftarrow \mathbf{E}^n, & \forall \mathbf{r}' \in \Omega, \\ \psi_{\mathbf{r}'_{i,0}}^{n+1} \leftarrow \psi^n, & \text{for } \mathbf{r}'_{i,0} \in \omega_i, \forall i \in [1, I], \\ \mathbf{P}_{\mathbf{r}'_{i,0}}^{n+1} \leftarrow \psi_{\mathbf{r}'_{i,0}}^{n+1}, & \text{for } \mathbf{r}'_{i,0} \in \omega_i, \forall i \in [1, I], \\ \nabla_{\mathbf{r}'}\psi_{\mathbf{r}'_{i,0}}^{n+1} \leftarrow \psi_{\mathbf{r}'_{i,0}}^{n+1} \text{ and Eq. (13),} & \text{for } \mathbf{r}'_{i,0} \in \omega_i, \forall i \in [1, I], \\ \nabla_{\mathbf{r}'}\mathbf{P}_{\mathbf{r}'_{i,0}}^{n+1} \leftarrow \nabla_{\mathbf{r}'}\psi_{\mathbf{r}'_{i,0}}^{n+1}, & \text{for } \mathbf{r}'_{i,0} \in \omega_i, \forall i \in [1, I], \\ \mathbf{P}_{\mathbf{r}'_j}^{n+1} \leftarrow \mathbf{P}_{\mathbf{r}'_{i,0}}^{n+1}, (\nabla_{\mathbf{r}'}n)(\mathbf{r}'_{i,0}) \text{ and } \nabla_{\mathbf{r}'}\mathbf{P}_{\mathbf{r}'_{i,0}}^{n+1}, & \forall \mathbf{r}'_j \in \omega_i, \text{ and } \forall i \in [1, I]. \end{array} \right.$$

This technique has not been computed yet, but constitutes a low cost approach to increase the size of the gas, with an order 2 precision. Note also that from another point of view it would be interesting to investigate a coupling of this approach with a local (in each Maxwell-cell) slowly varying envelope approximation (see Section 2).

3.4. Remarks on real 2-D boundary conditions and application to 3-D domains

Let us now discuss some ideas on the boundary condition problem for excited molecule TDSE's. The initial wavefunction ψ (initial state) support is located in the ‘‘Schrödinger computational domain center’’. Then the laser pulse interacts with the molecules and delocalizes the wavefunction (electrons and nuclei) whose support can become very large (discrete and continuum spectra). Numerically it means that it is necessary to discretize the TDSE's on a very large domain. To overcome this well known problem in numerical scattering theory, we have to find an adapted method to design boundary conditions. The usual idea to circumvent this difficulty is to reduce the computational domain and to impose some particular numerical boundary conditions on the bounded domain. It is well known that imposing Dirichlet or Neumann boundary conditions leads to important numerical oscillations and reflections on the boundary of the domain interacting with ‘‘physical’’ waves inside the domain. The one-dimensional case is detailed in [26] but are also discussed in [27]. We then propose to give some directions to extend the boundary conditions in realistic (that is above planar surfaces) two or three dimensions as singularities of a cubic 3-D domain lead us to construct truly multidimensional boundary conditions. In this goal let us recall some important results. Considering the 2-D problem (with $\mathbf{r} = (x, y)$ here).

$$\left\{ \begin{array}{l} i\partial_t u = -[\Delta_{\mathbf{r}} + V_c(\mathbf{r})]u, \quad \mathbf{r} \in \mathbb{R}^2, \\ u(\mathbf{r}, 0) = u_0(\mathbf{r}). \end{array} \right.$$

As in a 1-D case, we want to determine the Dirichlet–Neumann boundary conditions we then have to solve outside a compact domain Ω containing the supports of u_0 and V_c , the free particle equation:

$$i\partial_t u = -\Delta_{\mathbf{r}} u, \quad \mathbf{r} \in \Omega^C.$$

The solution is obtained using the Laplace transform in space (see [36]) and the Sommerfeld radiation condition that ensures uniqueness and positivity of the energy flux. It is well known that these conditions are nonlocal in space and in time. That is the

condition on each point of the boundary depends on all boundary points at all previous times. It is then computationally very complex to apply directly such a method. It is necessary to establish an appropriate numerical method effective in space and time or at least in time or in space. With this aim, we propose to use the approach of Antoine and Besse as a starting point. They were able to approximate (to order 3) by some differential operators Dirichlet–Neumann conditions. That is the spatial nonlocality is replaced by “local” differential operators even if the formulation remains nonlocal in time. In particular they proved in 2-D this nice theorem (see [2]):

Theorem 3.2. (See Antoine and Besse, '01.) *The TDSE with artificial boundary conditions of Dirichlet–Neumann type of order $m/2$ with $m \in \{1, \dots, 4\}$ is defined by the initial boundary value problem:*

$$\begin{cases} i \partial_t u(\mathbf{r}, t) + \Delta_{\mathbf{r}} u(\mathbf{r}, t) = 0, & (\mathbf{r}, t) \in \Omega \times \mathbb{R}_+^*, \\ \partial_{\mathbf{n}} u(\mathbf{r}, t) + T_{m/2} u(\mathbf{r}, t) = 0, & (\mathbf{r}, t) \in \Omega \times \mathbb{R}_+^*, \\ u(\mathbf{r}, 0) = u_0(\mathbf{r}), & \mathbf{r} \in \Omega, \end{cases}$$

where $T_{m/2}$ are pseudo-differential in time and differential in space operators given by:

$$\begin{cases} T_{1/2} u = e^{-i\pi/4} \partial_t^{1/2} u, & \partial\Omega \times \mathbb{R}_+^*, \\ T_1 u = T_{1/2} u + \frac{\kappa}{2} u, & \partial\Omega \times \mathbb{R}_+^*, \\ T_{3/2} u = T_1 u - e^{i\pi/4} \left(\frac{\kappa^2}{8} + \frac{1}{2} \Delta_{\partial\Omega} \right) I_t^{1/2} u, & \partial\Omega \times \mathbb{R}_+^*, \\ T_2 u = T_{3/2} u + i \left(\frac{\kappa^3}{8} + \frac{1}{2} \partial_s (\kappa \partial_s) + \frac{\Delta_{\partial\Omega} \kappa}{8} \right) I_t u, & \partial\Omega \times \mathbb{R}_+^*. \end{cases}$$

The operator $\Delta_{\partial\Omega}$ is the Laplace–Beltrami operator and κ is the local curvature of $\partial\Omega$. The pseudo-differential convolution $I_t^{1/2}$ and $\partial_t^{1/2}$ are defined by:

$$\partial_t^{1/2} u(t) = \frac{1}{\sqrt{t}} \frac{d}{dt} \int_0^t \frac{u(y)}{\sqrt{t-y}} dy, \quad I_t^{1/2} u(t) = \frac{1}{\sqrt{\pi}} \frac{d}{dt} \int_0^t \frac{u(y)}{\sqrt{t-y}} dy.$$

These conditions in the two-dimensional case allow them to reduce drastically the spurious reflexions on $\partial\Omega$ (see [3]). The extension of these formulas to the 3-D case is of course possible and is based on the Laplace transform in time of the TDSE, the resolution of the obtained Helmholtz equation under the Sommerfeld radiation condition and then by inverse Laplace transform. We then propose to combine these boundary conditions with the electric field interaction operator. In order to use the 2-D approach, we propose to work in cylindrical coordinates for the 3-D problem.

We assume here that the nuclei are fixed (Born–Oppenheimer approximation) and the potentials are set to zero. This assumption is only imposed for the sake of simplicity and has no consequence on the method as the extension can be deduced from [26]. In cylindrical coordinates and for fixed nuclei and for a polarized field in z , our equation becomes:

$$\begin{cases} \left(i \partial_t + \Delta_r + \frac{1}{r} \partial_r + \frac{1}{r^2} \Delta_{\theta} + \Delta_z + z \mathbf{E}(t) \right) v(r, \theta, z, t) = 0, & (r, \theta, z, t) \in \mathbb{R}^+ \times [0, 2\pi[\times \mathbb{R} \times \mathbb{R}_+^*, \\ v(r, \theta, z, 0) = v_0(r, \theta, z), & (r, \theta, z) \in \mathbb{R}^+ \times [0, 2\pi[\times \mathbb{R}. \end{cases}$$

Spatial variables are then $\theta \in [0, 2\pi]$, $r \in]0, R_{\max}[$ and $z \in [-z_{\max}, z_{\max}]$. We denote by Γ_{θ} and Γ_z and Γ_{-z} the following surfaces (see Fig. 15):

$$\begin{cases} \Gamma_{\theta} = \{ (r, \theta, z), \text{ such that } r = R_{\max}, \theta \in [0, 2\pi[, z \in [-z_{\max}, z_{\max}] \}, \\ \Gamma_z = \{ (r, \theta, z), \text{ such that } r \in]0, R_{\max}], \theta \in [0, 2\pi[, z = z_{\max} \}, \\ \Gamma_{-z} = \{ (r, \theta, z), \text{ such that } r \in]0, R_{\max}], \theta \in [0, 2\pi[, z = -z_{\max} \}. \end{cases}$$

Finally $\Gamma = \Gamma_{\theta} \cup \Gamma_{-z} \cup \Gamma_z$. The natural Dirichlet–Neumann boundary conditions (remark that $[\Delta_r, \Delta_z] = [\Delta_{\theta}, \Delta_z] = 0$) are then given by extension of formulas in [26] but also shortly discussed in [27]:

$$\begin{cases} -\partial_{\mathbf{n}_{\Gamma_{-z}}} v(r, \theta, z, t) = \sqrt{2} e^{i\pi/4} \int_0^t \frac{\partial_z u(r, \theta, z_{\Gamma_{-z}}, \tau)}{\sqrt{\pi(t-\tau)}} d\tau, & (r, \theta, z) \in \Gamma_{-z}, \\ -\partial_{\mathbf{n}_{\Gamma_z}} v(r, \theta, z, t) = \sqrt{2} e^{i\pi/4} \int_0^t \frac{\partial_z u(r, \theta, z_{\Gamma_z}, \tau)}{\sqrt{\pi(t-\tau)}} d\tau, & (r, \theta, z) \in \Gamma_z, \\ -\partial_{\mathbf{n}_{\Gamma_{\theta}}} v(r = R_{\max}, \theta, z, t) + T_{m/2} u(r = R_{\max}, \theta, z, t) = 0, & (r, \theta, z) \in \Gamma_{\theta}. \end{cases}$$

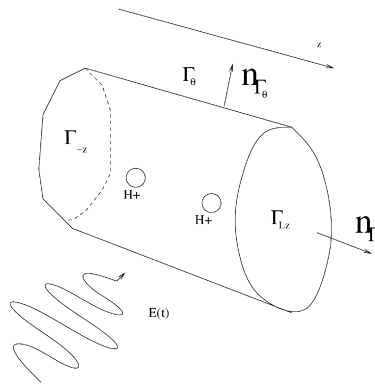


Fig. 15. 3-D domain for H₂⁺ with internuclear distance *R* in presence of laser pulse *E*(*t*).

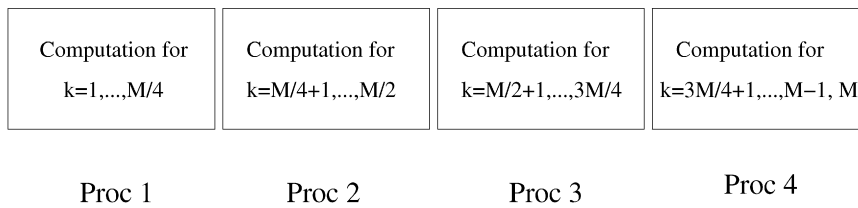


Fig. 16. Sampling for 4 processors.

In the particular case of a circular cylinder, the Laplace–Beltrami operator Δ_{Γ_θ} is given by Δ_θ . Note that numerically the key point is that we make terms $\partial_z u$ in the R.H.S. of the first two lines depend on the laser field (polarized in *z*) by an historical and local decomposition process of the temporal integral as described in [27] in the one-dimensional case.

4. Parallelization of the Maxwell–Schrödinger model

In this section we describe the parallelization proposed to make decrease the computational time for large physical systems.

4.1. Parallelization of the TDSE beyond Born–Oppenheimer approximation

The operator splitting proposed above induces a natural parallelization.

- Indeed, the “electronic” step of (9):

$$i \frac{\psi_{\mathbf{r}_j,k}^{n+1/2} - \psi_{\mathbf{r}_j,k}^n}{\Delta t_S} = -\frac{\Delta_{\mathbf{r}} \psi_{\mathbf{r}_j,k}^{n+1/2}}{4} + \frac{V_c}{2} \psi_{\mathbf{r}_j,k}^{n+1/2} - \frac{\Delta_{\mathbf{r}} \psi_{\mathbf{r}_j,k}^n}{4} + \left(\frac{V_c}{2} + \mathbf{r} \cdot \mathbf{E}^n \psi_{\mathbf{r}_j,k}^n \right) \psi_{\mathbf{r}_j,k}^n,$$

has to be computed for all $k \in \{1, \dots, M\}$ (that is for all $R_k = k\Delta R$ in $]0, R_\infty[$). But as the differential Laplace operator is independent of *R* (then of *k*), we have to solve *M* independent sparse linear systems. Each numerical computation is done using a Krylov iterative method with initial data depending on *k*:

$$P \psi_k^{n+1/2} = Q \psi_k^n, \quad k \in \{1, \dots, M\},$$

where *P* and *Q* are matrices of $M_{\mathcal{N},\mathcal{N}}(\mathbb{C})$, with \mathcal{N} the number of points in the electronic grid. We then sample $\{1, \dots, M\}$ on the nodes of the parallel computer (see Fig. 16). In term of algorithmic complexity each linear system computation (with preconditioning) is of order $O(\mathcal{N}^{3/2})$. As the number of computations is equal to *M*, the total algorithmic complexity at each iteration is given by $O(M\mathcal{N}^{3/2})$. By independence of the linear systems, and for a number of processors equal to *p*, each processor computes $O(M\mathcal{N}^{3/2}/p)$ operations.

- Considering now the parallelization of the nuclear step of (9), $k \in \{1, \dots, M\}$:

$$i \frac{\psi_{\mathbf{r}_j,k}^{n+1} - \psi_{\mathbf{r}_j,k}^{n+1/2}}{\Delta t_S} = -\frac{\Delta_R \psi_{\mathbf{r}_j,k}^{n+1}}{2m_p} + \frac{V_i}{2} \psi_{\mathbf{r}_j,k}^{n+1} - \frac{\Delta_R \psi_{\mathbf{r}_j,k}^{n+1/2}}{2m_p} + \frac{V_i}{2} \psi_{\mathbf{r}_j,k}^{n+1/2}, \quad \forall \mathbf{r}_j.$$

The process is different due to the fact that applying a similar parallelization than above would be very costly in 3-D (as the number of cells is of order \mathcal{N}). We propose an approach based on the fact that numerically the cell number in the *R*-grid is

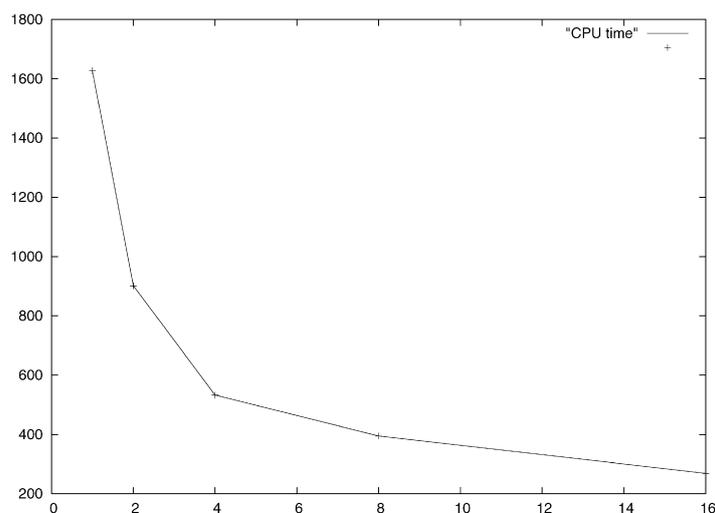


Fig. 17. Speed-up: 1 → 16 processors.

much smaller than in the electronic grid as the nuclear equation is a one-dimensional PDE. The numerical nuclear step can then be summarized by the compact form:

$$H \psi_{\mathbf{r}_j}^{n+1} = K \psi_{\mathbf{r}_j}^{n+1/2},$$

where H and K are M -row and column complex matrices, with M defined above. We then propose to compute and to store the constant discrete operator $H^{-1}K$. This process has to be done only one time. We are then led to compute \mathcal{N} matrix–vector products to deduce the global wavefunction. The natural parallelization then consists in the well known parallelization of the matrix–vector product $H^{-1}K \times \psi^{n+1/2}$. The use of this technique implies an adapted numerical code design that is not detailed here.

In Fig. 17, we present the real computational time with respect to the number of processors. The simulations run on a computer of 576 nodes Dell 1425SC (1152 CPU Intel Xeon, 3.6 GHz) 8 GB RAM/node with infinite band network 4X. The baby-benchmark consists in a one-dimensional laser–molecule interaction with 100 points in the “electronic”-grid, 100 points in the “nuclear”-grid.

4.2. Parallelization of the polarization computation in the Born–Oppenheimer approximation

Many approaches are possible to parallelize the Maxwell–Schrödinger model. One of the most effective is as follows. To simplify the presentation let us suppose that the Maxwell-grid possesses N cells and that we solve N TDSE’s (one by Maxwell-cell) with a code running on N processors. We also suppose in this paragraph that the Maxwell-domain is not “very large” so that it is possible to solve the Maxwell’s equations on one single processor. At each temporal Maxwell iteration, each processor solves one single TDSE, and computes the corresponding polarization. Then it sends it to the root processor. Then the root processor can solve the non-homogeneous Maxwell’s equations (recall that in our configuration (small Maxwell-domain) the CPU cost of the Maxwell’s equation computation is negligible compared to the TDSE computation cost). Then the root processor sends to the slaves the updated electric field (this process is summarized in Fig. 18). Such a simple parallelization allows us to obtain a very good speed-up. Note also that the data are distributed between the computer nodes allowing to consider a large number of molecules with sufficiently large spatial grids. Fig. 19 represents for a given mesh: in abscissa the number of TDSE’s (4, 16, 64, 256 TDSE’s) to solve also equal to the number of processors (one equation by processor) and in ordinate the real time for the 3-D code to solve the corresponding Maxwell–TDSE model. The ideal configuration would be “real time=constant”, corresponding to a speed-up equal to the number of processors. Note also that the parallelization is almost totally independent of the way we solve numerically the Schrödinger and Maxwell’s equations.

We present now another approach used for large 3-D Maxwell-domains. In this case, the parallelization we propose is also based on a domain decomposition for the Maxwell’s equation computation. Let us suppose that we have N processors and N_2 TDSE’s to solve. We make a partition of the Maxwell domain in $N_1 = N - N_2$ subdomains. In practice, $N_1 \ll N_2$ as the TDSE computations are more costly than the Maxwell ones. Suppose for instance that the gas is totally located in the \bar{N} th subdomain ($\bar{N} \leq N_1$). The computational steps become:

- the Maxwell’s equations are solved with processors $\{1, \dots, N_1\}$ on each subdomain with message passing at subdomain interfaces.

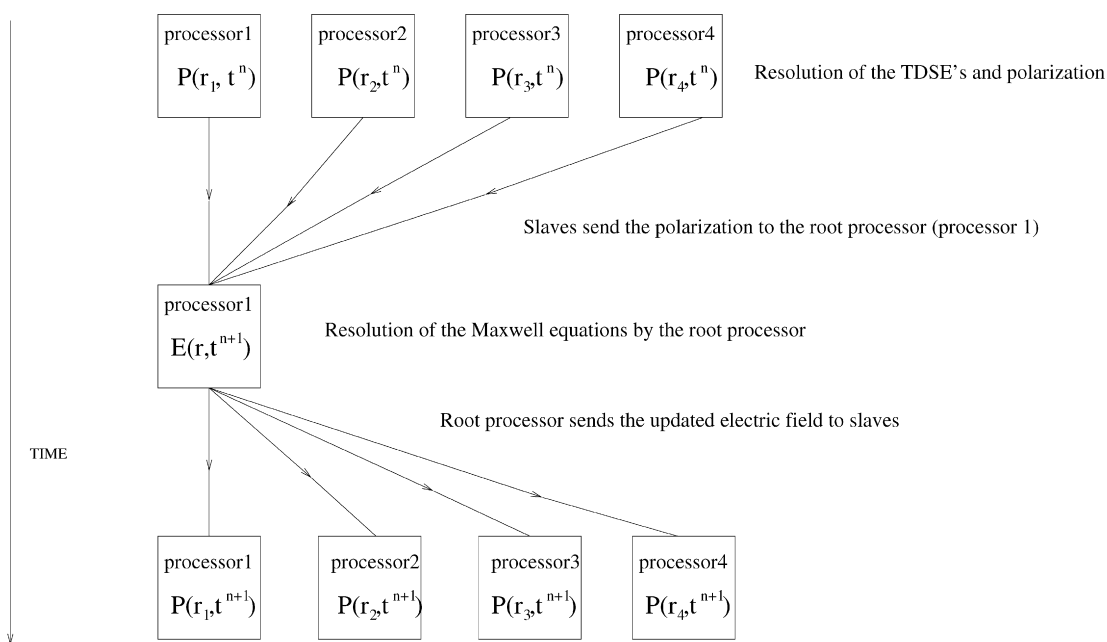


Fig. 18. Parallelization for 4 TDSE's.

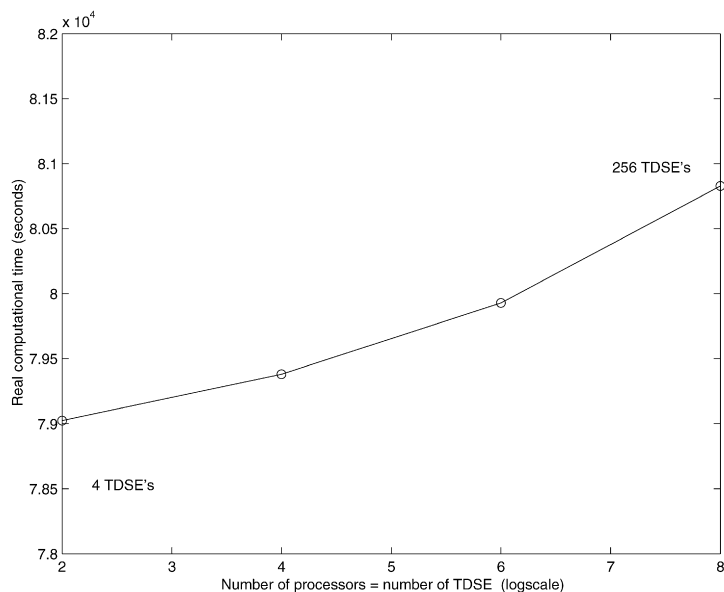


Fig. 19. Computation of the 3-D Maxwell–TDSE with one TDSE per processor. In ordinate the real time (in seconds) necessary for the numerical computation.

- the processor \bar{N} sends the corresponding electric field to the molecules of the gas, that is to processors $\{N_1 + 1, \dots, N\}$.
- independently, the N_2 TDSE's are solved, and give the associated polarization.
- each processor $\{N_1 + 1, \dots, N\}$ sends to the \bar{N} th processor its computed polarization.

The temporal process consists in two sub-iterations: computing the Maxwell's equations on N_1 processors (first temporal sub-iteration) and then computing the TDSE's on N_2 processors (second temporal sub-iteration). See Figs. 20 and 21. Note also that such a decomposition allows us to distribute the memory between the nodes of the parallel computer, and is highly scalable as the TDSE's computations are totally independent. This parallelization has been used for the largest computations (see numerical results section).

5. Numerical examples

In this part we present some results obtained with the numerical and parallel approaches introduced above. In the following experiments the nuclei motion is not included and we have imposed absorbing boundary conditions as here, we do not focus on the

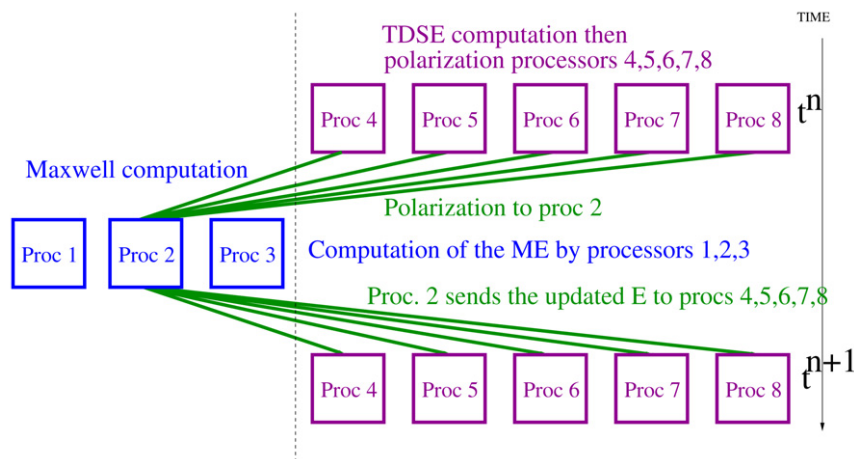


Fig. 20. Parallelization approach for 5 TDSE's and 8 processors—1.

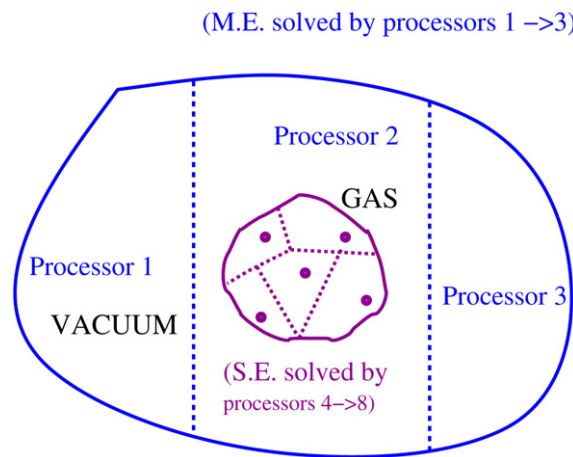


Fig. 21. Parallelization approach for 5 TDSE's and 8 processors—2.

plasma effects. We consider Ti:sapphire pulses with intensity $I \sim 10^{14} \text{ W/cm}^2$ or $I \sim 4 \times 10^{14} \text{ W/cm}^2$ at 800 nm interacting with a H_2^+ -gas. The aim is to validate the model we have proposed and to show the kind of simulations the model allows.

5.1. Maxwell 1-D–Schrödinger 1-D

The problem we first consider consists in the Maxwell–Schrödinger coupling in 1-D. We suppose here that the molecules are aligned. The first result, Fig. 22, represents for a 1-D computation, the harmonic orders contained in the transmitted electric field $\hat{E}(\omega)$ of intensity $|\hat{E}(\omega)|^2 (N\omega_0)$, with ω_0 the incident laser frequency), for a few-cycle (2–3 cycles) laser pulse propagating in a H_2^+ medium of length equal from 14 nm (corresponding to 1 TDSE), to 28.7 μm (2048 TDSE's) with an inter-nuclear distance $R = 2$. Note that we obtain a linear scaling of the low order harmonic intensities, when we increase the domain length, as expected for such a coherent process [16,17] and as observed experimentally. Note also that the seventh harmonic is particularly excited as remarked in numerous computations for $R = 2$. This makes us remark that NLSE's or NLME's are absolutely not adapted here as usually only small order harmonics are considered in these models. In this case, as the density is very small (10 Torr, that is $\sim 3.54 \times 10^{17} \text{ mol/cm}^3$) the attopulses shape is a little modified (only linearly amplified) by the medium. In contrast for a much larger molecular density ($\sim 10^{20} \text{ mol/cm}^3$, with the same data than above and $R = 2$) we observe a modification on Fig. 23 of the linear scaling even for low order harmonic intensities (see, for instance, the seventh harmonics). This phenomenon is of particular interest for applications and for the medium response understanding.

5.2. Maxwell 1-D–Schrödinger 3-D

The second numerical result, Fig. 24, represents the transmitted electric field harmonics (squared) for a 3-D computation, with a 5-cycle pulse propagation in a H_2^+ media of length respectively equal to 4 nm (corresponding to 1 TDSE's), 15 nm (corresponding to 4 TDSE's), 60 nm (16 TDSE's), 240 nm (64 TDSE's). The pressure is here equal to 640 Torr. The code was run during approx-

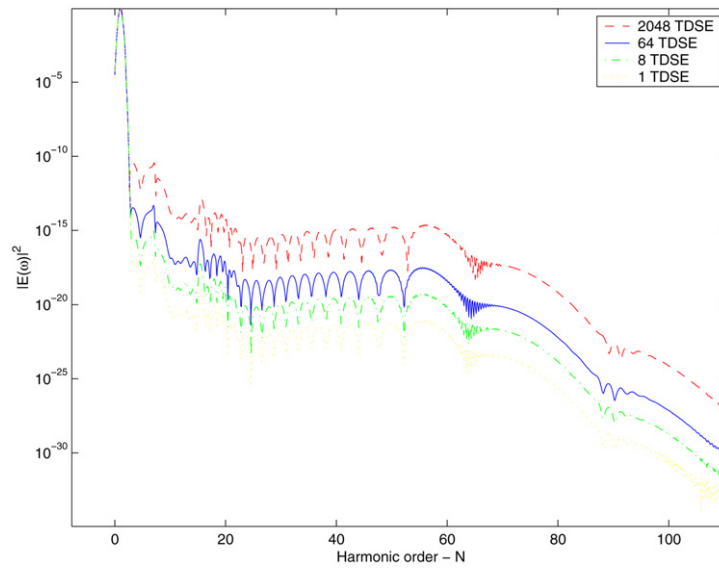


Fig. 22. $|\hat{E}(\omega)|^2$, for 14 nm (1 molecule), 112 nm (8 molecules), 896 nm (64 molecules) and 28.7 μm (2048 molecules) and $n_0 \sim 3.54 \times 10^{17}$ mol/cm³ in 1-D. In abscissa: harmonic order N , with $\omega = N\omega_0$ and ω_0 incident electric field frequency.

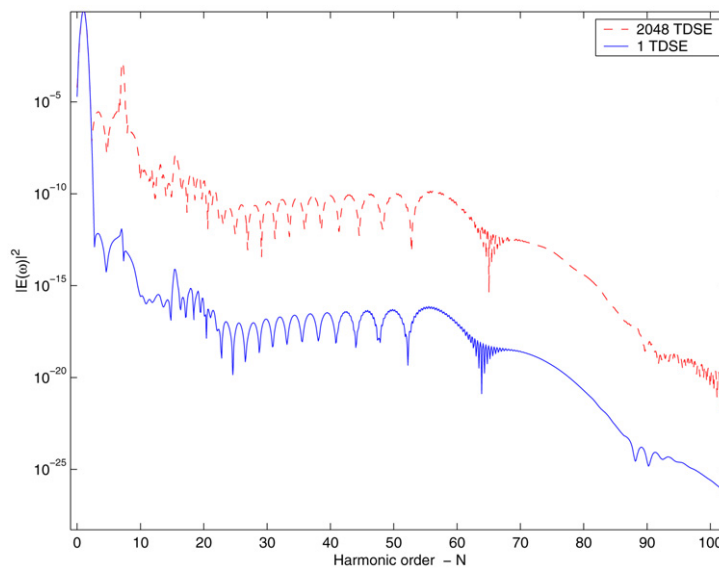


Fig. 23. $|\hat{E}(\omega)|^2$, for 2 nm (1 molecule) and 4 μm (2048 molecules) and $n_0 \sim 10^{20}$ mol/cm³ in 1-D. In abscissa: harmonic order N , with $\omega = N\omega_0$ and ω_0 incident electric field frequency.

imatively 22 hours, respectively, on 1, 4, 16 and 64 Xeon (Intel) processors (see www.ccs.usherbrooke.ca/mammoth). Again, we remark that the computation gives us a linear scaling for the low order harmonics with respect to the propagation length. These results show also the high order harmonic generation by the electric field acting on the H_2^+ molecules and the high intensity of some of these harmonics as a result of nonlinear non-perturbative laser–molecule interaction. This observation confirms again the necessity for the use of our Maxwell–Schrödinger model instead of perturbative NLSE or NLME models to study intense ultrashort laser pulse behaviors. Our model can then be, for instance, an efficient tool for the filamentation study [30]. Indeed, this multidimensional phenomenon is usually treated using nonlinear TDSE with a plasma term modeled with a nonlinear function of the electric field.

Finally, note that by filtering around high intense harmonics it is also possible to create shorter pulses (much higher frequency as $\Delta t \times \Delta \omega \sim 1$) than the incident one. See for instance that, the 70th harmonics is relatively intense allowing to create by filtering an “intense” pulse of frequency 70 times larger than the incident laser one [1]. The second test, Fig. 25, is at $R = 2$ with $I \sim 4 \times 10^{14}$ W/cm² and $n_0 \sim 10^{20}$ mol/cm³. We observe again that as expected the cut-off is located around $I_p + 3.17U_p$ that is in this case the 30th harmonic. As we can see on these results the most excited harmonics depend on the inter-nuclear distance (the 7th for $R = 2$, and the 3th for $R = 3.2$). This then pleads to take into account nuclei motion and then to go beyond the Born–Oppenheimer approximation, what is possible with our model, but not with nonlinear Schrödinger models for instance.

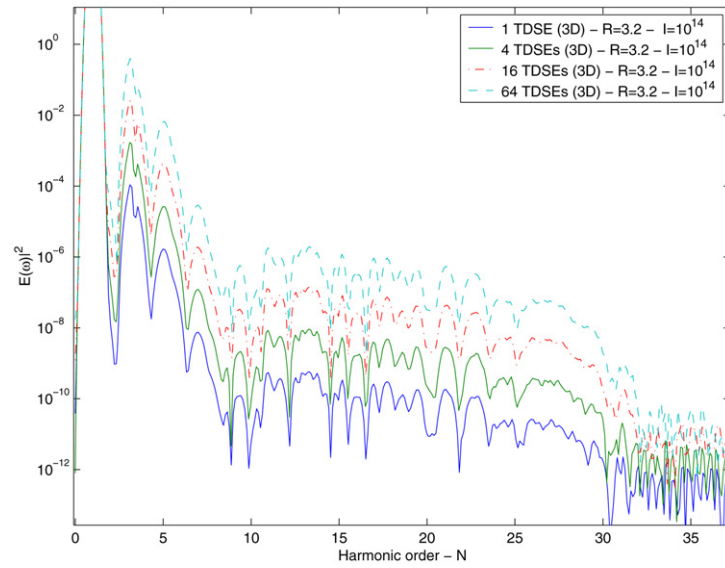


Fig. 24. $|\hat{E}(\omega)|^2$, for 4 nm (1 molecules), for 15 nm (4 molecules), 60 nm (16 molecules), 240 nm (64 molecules) in 3-D. In abscissa: harmonic order N , with $\omega = N\omega_0$, and ω_0 incident electric field frequency.

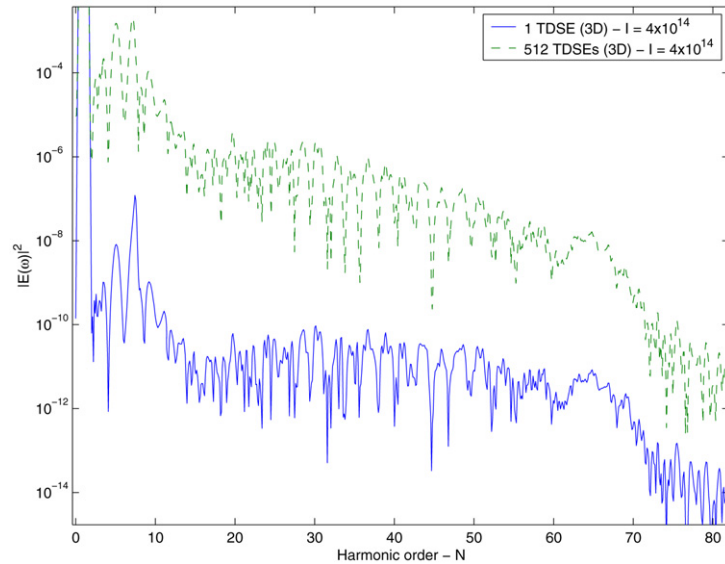


Fig. 25. $|\hat{E}(\omega)|^2$, for 4 nm (1 molecules), 60 nm (16 molecules), 2.05 μm (512 molecules) in 3-D. In abscissa: harmonic order N , with $\omega = N\omega_0$, and ω_0 incident electric field frequency.

5.3. Maxwell 3-D–Schrödinger 3-D

The next benchmark is the computation of our 3-D Maxwell–Schrödinger model with the following data: the Maxwell domain is a cubic box $[0, 2.1 \times 10^5]^3$ (in atomic units, that is approximately $10 \times 10 \times 10 \mu\text{m}^3$) with an uniform grid $\Delta x'_M = \Delta y'_M = \Delta z'_M = 750$ a.u. (allowing to consider rigorously at least the 20 first transmitted electric field harmonics). The TDSE's have been solved using the Crank–Nicolson scheme presented above with grid steps of length $\Delta x_S = \Delta y_S = \Delta z_S = 0.2$ a.u. The initial state for molecules has been computed exactly in the Born–Oppenheimer approximation with $R = 3.2$ a.u. At such distance and $\lambda = 800$ nm, there is a three-photon ionization resonance for the $1\sigma_g - 1\sigma_u$ excitation [15]. The electric field propagated in vacuum, is presented in Fig. 27. We then study the effect of a gas on multidimensional electric field taking into account ionization and HHG. The circular electric field propagates in the vacuum then through a H_2^+ -gas of volume equal to $3750 \times 3750 \times 7500$ a.u.³ The number of 3-D TDSE's to solve is equal to $5 \times 5 \times 10 = 250$. The physical computational time is 632 a.u. that is ~ 15 fs. We represent in Fig. 28 the difference between the electric field propagating in the gas and in vacuum, at z fixed in the middle of the gaseous medium. We clearly observe the reflected wave. One of our main goals is the numerical observation of filaments: intense and high frequency laser pulses propagating in a dense medium (typically a Gaussian beam) are focalized by Kerr effect, and then

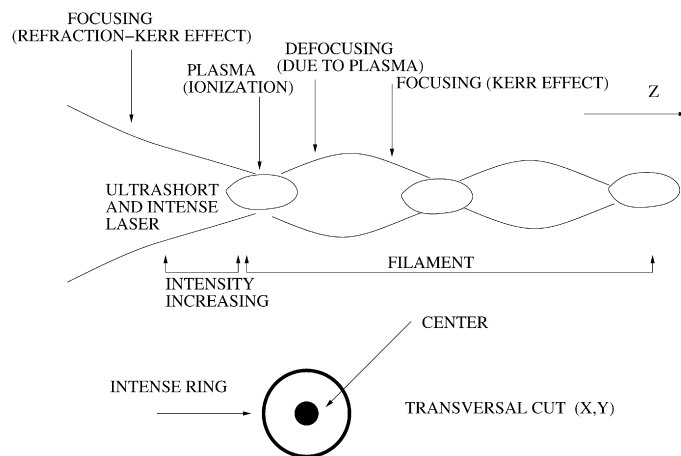


Fig. 26. Filamentation.

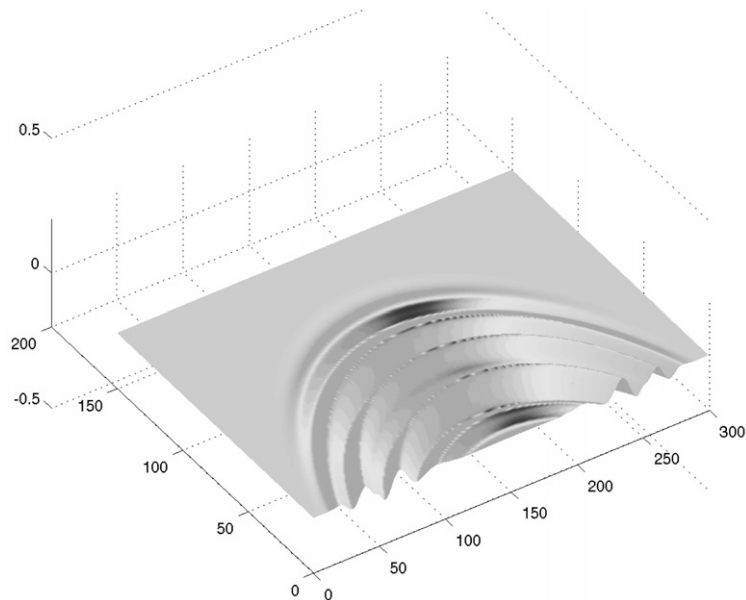


Fig. 27. Transmitted electric field in vacuum.

defocused by the plasma, due to electron ionization. Kerr effect re-focuses the beam and so on. Some so-called filaments are then created and can propagate over very large distances (meters), see Fig. 26. This phenomenon is currently an intensive source of research because of numerous possible applications in engineering (polluted gas detection and composition, lightning control, air communications, etc.) and in theoretical physics. As it would be necessary to solve thousands of 3-D TDSE's, at this point we are not able to obtain numerically these filaments. Note that for few-cycles pulses free electrons remain inside the computational domain, it is then not necessary to impose sophisticated boundary conditions in this case. However an approach coupling 1-D TDSE with 3-D Maxwell's equations is in progress and could lead to observe this phenomenon. Currently filaments are numerically observe with rough nonlinear Schrödinger models containing an approximate nonlinear term modeling the plasma effects. With such a Maxwell-Schrödinger model we will be able to very precisely understand this phenomenon and possibly will give some ideas for its control.

6. Conclusion

In this paper we have presented a Maxwell-Schrödinger model for time dependent laser-matter interaction and some aspects of its numerical computation in 1-D and 3-D. The model we have introduced is the first to be nonperturbative (no expansion with respect to a small parameter) vectorial, multidimensional, going beyond slowly varying envelope approximation and that takes ionization into account. We then go far beyond usual nonlinear Maxwell or Schrödinger models commonly used in the framework of laser-matter interaction. In the model the coupling between the laser and the gas is ensured by the polarization corresponding to

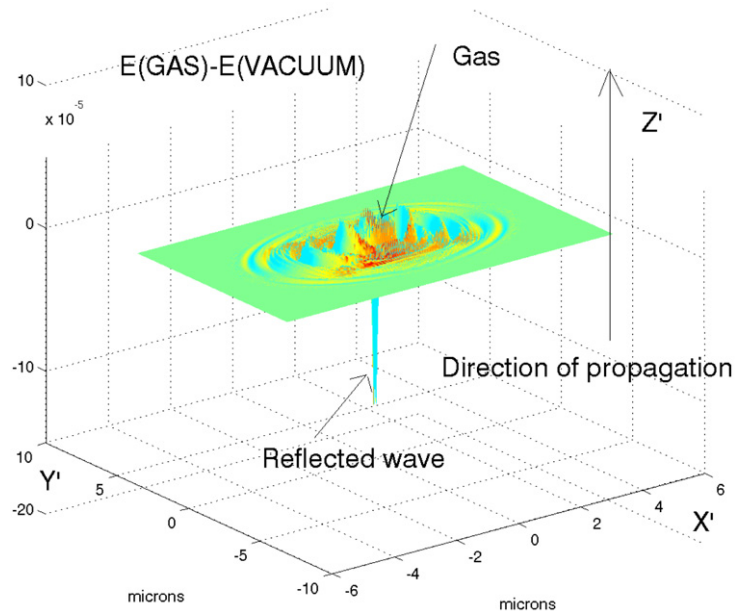


Fig. 28. Difference between the electric field for a 3-D- Maxwell–Schrödinger propagation in the gas and in vacuum (250 TDSE’s).

the quantum gas reaction to the intense laser pulse. This new *ab initio* approach is a new step to understand more fundamentally the laser–molecule interactions, for instance, the behavior of the HHG process for many molecules. To be able to solve numerically this complex model, we have proposed some efficient methods to manage, multiple scales (polarization computation, for instance). Based on these elements a numerical code has been developed, with an effective parallel approach, which allows us to study the spatial structure of the propagated pulses (scalability of harmonic intensity when the propagation length increases) and seems a good tool to study the filamentation phenomena. Numerical simulations were obtained so far only for fixed R although some remarks on numerical TDSE with moving nuclei have also been addressed. Remark that computations with our Maxwell–Schrödinger code via Eqs. (5), (7), (6) require Peta-Byte super-computers. In a future work, spectral approaches will be considered for the Maxwell’s equation computation to enable us to capture with high precision, higher than in this work, transmitted electric field harmonics. New phenomena as filamentation will also be deeply studied using our model.

Appendix A. Proof of Theorem 2.1

Proof. In the following we will denote by \mathcal{E} the laser operator:

$$\mathcal{E} : (\mathbf{r}, R, t) \mapsto \mathcal{E}(\mathbf{r}, R, t) = \chi(\mathbf{r}, R) \cdot \mathbf{E}(t).$$

In a first time we regularize the potentials, defining

$$V_c^\epsilon = -\frac{1}{\sqrt{\epsilon^2 + x^2 + (y - R/2)^2 + z^2}} - \frac{1}{\sqrt{\epsilon^2 + x^2 + (y + R/2)^2 + z^2}}, \quad V_i^\epsilon = -\frac{1}{\sqrt{\epsilon^2 + R^2}}.$$

We then have $|V_c^\epsilon| \leq |V_c|$ and $|V_i^\epsilon| \leq 1/R$ and $\partial_t V_c^\epsilon = \partial_t V_i^\epsilon = 0$. Then

$$i \partial_t \psi^\epsilon(\mathbf{r}, R, t) = \left[-\frac{1}{2} \Delta_{\mathbf{r}} + V_c^\epsilon(\mathbf{r}, R) + \chi(\mathbf{r}, R) \cdot \mathbf{E}(t) + V_i^\epsilon(R) \right] \psi^\epsilon(\mathbf{r}, R, t).$$

As remarked above there exists a unique $\psi^\epsilon \in C^0(0, T; H^1 \cap H_1)$ as $V_i^\epsilon, V_c^\epsilon, \chi(\mathbf{r}, R) \cdot \mathbf{E}(t) \in L^\infty(0, T; C_b^2(\mathbb{R}^4))$. We now search for an estimation in H_1 of ψ^ϵ . First recall that:

$$\|\psi^\epsilon(t)\|_{H^1 \cap H_1}^2 = \int_{\mathbb{R}^4} |\nabla_{\mathbf{r}} \psi^\epsilon|^2 + |\nabla_R \psi^\epsilon|^2 + (1 + \|(\mathbf{r}, R)^T\|_2^2) |\psi^\epsilon|^2.$$

Then there exists a constant $M_p > 0$ ($= 1$, for instance, as $m_p > 1$) such that:

$$\int_{\mathbb{R}^4} \frac{|\nabla_{\mathbf{r}} \psi^\epsilon|^2}{2} + \frac{|\nabla_R \psi^\epsilon|^2}{m_p} + (1 + \|(\mathbf{r}, R)^T\|_2^2) |\psi^\epsilon| \leq M_p \|\psi^\epsilon(t)\|_{H^1 \cap H_1}^2. \tag{A.1}$$

The main difficulty consists in finding a positive constant C such that:

$$\|\psi^\epsilon(t)\|_{H^1 \cap H_1}^2 \leq C \|\psi_0\|_{H^1 \cap H_1}^2. \tag{A.2}$$

Supposing (A.2) is true and using a compactness argument, there exists a sequence ϵ_n such that

$$\psi^{\epsilon_n} \rightharpoonup_{n \rightarrow \infty}^* u \quad \text{in } L^\infty(0, T; H^1 \cap H_1).$$

We finally get

$$\|\psi(t)\|_{H^1 \cap H_1}^2 \leq C \|\psi_0\|_{H^1 \cap H_1}^2.$$

That proves the existence of a solution in the set described above.

In order to obtain estimation (A.2) it is necessary to have an estimation of

$$\frac{d}{dt} \int_{\mathbb{R}^4} (1 + \|(\mathbf{r}, R)^T\|_2) |\psi^\epsilon|^2, \quad \text{and} \quad \frac{d}{dt} \int_{\mathbb{R}^4} \frac{|\nabla_{\mathbf{r}} \psi^\epsilon|^2}{2} + \frac{|\nabla_R \psi^\epsilon|^2}{m_p}.$$

With this aim and as proposed in [10], we multiply the TDSE by $(1 + \|(\mathbf{r}, R)^T\|_2) \bar{\psi}^\epsilon$ we integrate on \mathbb{R}^4 and we take the imaginary part:

$$\frac{d}{dt} \int_{\mathbb{R}^4} (1 + \|(\mathbf{r}, R)^T\|_2) |\psi^\epsilon|^2 = \text{Im} \int_{\mathbb{R}^4} \nabla_{\mathbf{r}} [\|(\mathbf{r}, R)^T\|_2 \bar{\psi}^\epsilon] \frac{\nabla_{\mathbf{r}} \psi^\epsilon}{2} + \nabla_R [\|(\mathbf{r}, R)^T\|_2 \bar{\psi}^\epsilon] \frac{\nabla_R \psi^\epsilon}{m_p}.$$

We easily obtain by derivation and Cauchy–Schwarz

$$\frac{d}{dt} \int_{\mathbb{R}^4} (1 + \|(\mathbf{r}, R)^T\|_2) |\psi^\epsilon|^2 \leq \frac{1}{2} \int_{\mathbb{R}^4} \|(\mathbf{r}, R)^T\|_2 |\psi^\epsilon|^2 + \frac{|\nabla_{\mathbf{r}} \psi^\epsilon|^2}{2} + \frac{|\nabla_R \psi^\epsilon|^2}{m_p}.$$

The same manner we multiply by $\partial_t \bar{\psi}^\epsilon$ we take the real part and we integrate over \mathbb{R}^4 . That is

$$0 = \int_{\mathbb{R}^4} \text{Re} \left(-\frac{\partial_t \bar{\psi}^\epsilon \Delta_{\mathbf{r}} \psi^\epsilon}{2} - \frac{\partial_t \bar{\psi}^\epsilon \Delta_R \psi^\epsilon}{m_p} + V_c^\epsilon \psi^\epsilon \partial_t \bar{\psi}^\epsilon + V_i^\epsilon \psi^\epsilon \partial_t \bar{\psi}^\epsilon + \mathcal{E} \psi^\epsilon \partial_t \bar{\psi}^\epsilon \right). \tag{A.3}$$

Then

$$\begin{aligned} \frac{1}{2} \int_{\mathbb{R}^4} \partial_t \frac{|\nabla_{\mathbf{r}} \psi^\epsilon|^2}{2} + \partial_t \frac{|\nabla_R \psi^\epsilon|^2}{m_p} &= \frac{1}{2} \int_{\mathbb{R}^4} (V_c^\epsilon + V_i^\epsilon + \mathcal{E}) \partial_t |\bar{\psi}^\epsilon|^2 \\ &= \frac{d}{2 dt} \int_{\mathbb{R}^4} (V_c^\epsilon + V_i^\epsilon + \mathcal{E}) |\psi^\epsilon|^2 - \frac{1}{2} \int_{\mathbb{R}^4} \partial_t \mathcal{E} |\psi^\epsilon|^2. \end{aligned}$$

Then trivially there exists a constant C_2

$$\int_{\mathbb{R}^4} \partial_t \mathcal{E} |\psi^\epsilon|^2 \leq C_2 \left\| \frac{\partial_t \mathcal{E}}{1 + \|(\mathbf{r}, R)^T\|_2} \right\|_{L^\infty} \|\psi^\epsilon\|_{H^1}^2.$$

We then obtain the following estimate:

$$\frac{d}{dt} \int_{\mathbb{R}^4} \frac{|\nabla_{\mathbf{r}} \psi^\epsilon|^2}{2} + \frac{|\nabla_R \psi^\epsilon|^2}{m_p} \leq \frac{1}{2} \int_{\mathbb{R}^4} (V_c^\epsilon + V_i^\epsilon + \mathcal{E}) \partial_t |\psi^\epsilon|^2 + \frac{1}{2} \left\| \frac{\partial_t \mathcal{E}}{1 + \|(\mathbf{r}, R)^T\|_2} \right\|_{L^\infty} \|\psi^\epsilon\|_{H^1}^2. \tag{A.4}$$

Then setting:

$$E_{m_p}^\epsilon(t) = \frac{d}{dt} \int_{\mathbb{R}^4} \frac{|\nabla_{\mathbf{r}} \psi^\epsilon|^2}{2} + \frac{|\nabla_R \psi^\epsilon|^2}{m_p} + \int_{\mathbb{R}^4} (1 + \|(\mathbf{r}, R)^T\|_2) |\psi^\epsilon|^2,$$

and because of (A.3) and (A.4) we have:

$$\begin{aligned} \frac{d}{dt} E_{m_p}^\epsilon(t) &\leq \frac{1}{2} \int_{\mathbb{R}^4} \|(\mathbf{r}, R)^T\|_2 |\psi^\epsilon|^2 + \frac{1}{2} \int_{\mathbb{R}^4} \frac{|\nabla_{\mathbf{r}} \psi^\epsilon|^2}{2} + \frac{|\nabla_R \psi^\epsilon|^2}{m_p} \\ &\quad + \frac{d}{2dt} \int_{\mathbb{R}^4} (V_c^\epsilon + V_i^\epsilon + \mathcal{E}) |\psi^\epsilon|^2 + C_2 \left\| \frac{\partial_t \mathcal{E}}{1 + \|(\mathbf{r}, R)^T\|_2} \right\|_{L^\infty} \|E_{m_p}^\epsilon(t). \end{aligned}$$

As $\psi^\epsilon \in H_1$ and because of (A.3), there exists a positive constant C_3 such that:

$$\frac{d}{dt} E_{m_p}^\epsilon(t) \leq \frac{d}{dt} \int_{\mathbb{R}^4} (V_c^\epsilon + V_i^\epsilon + \mathcal{E}) |\psi^\epsilon|^2 + C_3 \left[1 + \left\| \frac{\partial_t \mathcal{E}}{1 + \|(\mathbf{r}, R)^T\|_2} \right\|_{L^\infty} \right].$$

By integration we have

$$\begin{aligned} E_{m_p}^\epsilon(t) &\leq \int_{\mathbb{R}^4} (V_c^\epsilon + V_i^\epsilon + \mathcal{E}(0)) |\psi^\epsilon(0)|^2 + \int_{\mathbb{R}^4} (V_c^\epsilon + V_i^\epsilon + \mathcal{E}(t)) |\psi^\epsilon(t)|^2 \\ &\quad + C_3 \int_0^t \left[1 + \left\| \frac{\partial_t \mathcal{E}}{1 + \|(\mathbf{r}, R)^T\|_2} \right\|_{L^\infty} \right] E_{m_p}^\epsilon(s) ds + E_{m_p}^\epsilon(0). \end{aligned}$$

As

$$\int_{\mathbb{R}^4} (V_c^\epsilon + V_i^\epsilon) |\psi^\epsilon(t)|^2 \leq \int_{\mathbb{R}^4} (V_c + V_i) |\psi^\epsilon(t)|^2 \leq \left(\int_{\mathbb{R}^4} (V_c + V_i)^2 |\psi^\epsilon(t)|^2 \right)^{1/2} \left(\int_{\mathbb{R}^4} |\psi^\epsilon(t)|^2 \right)^{1/2}.$$

By definition of V_i and V_c and applying an Hardy inequality, there exists a positive constant C_4 such that:

$$\int_{\mathbb{R}^4} |\psi^\epsilon(t)|^2 (V_c + V_i)^2 \leq 2 \int_{\mathbb{R}^4} |\psi^\epsilon(t)|^2 (V_c^2 + V_i^2) \leq 8 \int_{\mathbb{R}^4} |\nabla_{\mathbf{r}} \psi^\epsilon|^2 + |\nabla_R \psi^\epsilon|^2 \leq D \|\nabla_{\mathbf{r}, R} \psi^\epsilon\|_{L^2(\mathbb{R}^4)}.$$

So that, by the classical equality $\|\psi_0\|_{L^2}^2 = \|\psi^\epsilon\|_{L^2}^2$,

$$\int_{\mathbb{R}^4} (V_c^\epsilon + V_i^\epsilon) |\psi^\epsilon|^2 \leq \frac{C_4}{2} \|\nabla_{\mathbf{r}, R} \psi^\epsilon\|_{L^2(\mathbb{R}^4)} + \frac{C_4}{2} \|\psi_0\|_{L^2(\mathbb{R}^4)}. \tag{A.5}$$

Now as $E \in L^\infty(0, T)$ and $\chi \in C_b^2(\mathbb{R}^4)$

$$\int_{\mathbb{R}^4} \mathcal{E}(t) |\psi^\epsilon|^2 \leq \left\| \frac{\mathcal{E}}{1 + \|(\mathbf{r}, R)^T\|_2} \right\|_{L^\infty(0, T; \mathbb{R}^4)} \|\psi^\epsilon(t)\|_{H^1}^2 \tag{A.6}$$

and because of (A.1):

$$E_{m_p}^\epsilon(0) \leq M_p \|\psi_0\|_{H^1 \cap H_1}^2$$

and by definition of V_c and V_i there exists a positive constant C_5 such that

$$\int_{\mathbb{R}^4} (V_c^\epsilon + V_i^\epsilon + \mathcal{E}(0)) |\psi_0|^2 \leq C_5 \|\psi_0\|_{H^1 \cap H_1}^2. \tag{A.7}$$

So that (6), (A.5)–(A.7) lead to the existence of two positive constants C_6 and C_7 such that:

$$\|\psi^\epsilon(t)\|_{H^1 \cap H_1}^2 \leq C_6 \|\psi_0\|_{H^1 \cap H_1}^2 + C_7 \int_0^t \left[1 + \left\| \frac{\partial_t \mathcal{E}}{(1 + \|(\mathbf{r}, R)^T\|_2)^2} \right\|_{L^\infty(0, T; \mathbb{R}^4)} \right] \|\psi^\epsilon(s)\|_{H^1 \cap H_1}^2 ds.$$

We then apply the Gronwall inequality that leads to the existence of a positive constant C_I such that:

$$\|\psi^\epsilon(t)\|_{H^1 \cap H_1}^2 \leq C_I \exp \left(\int_0^t \left(1 + \left\| \frac{\partial_t \mathcal{E}}{1 + \|(\mathbf{r}, R)^T\|_2} \right\|_{L^\infty(0, T; \mathbb{R}^4)} \right) \|\psi^\epsilon(s)\|_{H^1 \cap H_1}^2 ds \right) \|\psi_0\|_{H^1 \cap H_1}^2.$$

Now as $\partial_t E \in L^1(0, T)$, there exists a constant C such that (A.2) occurs. The uniqueness is based on the same arguments than [10] again using a Gronwall inequality. \square

References

- [1] P. Agostini, L.-F. DiMauro, The physics of attosecond light pulses, *Rep. Prog. Phys.* 67 (813) (2004).
- [2] X. Antoine, C. Besse, Unconditionally stable discretization schemes of non-reflecting boundary conditions for the one-dimensional Schrödinger equation, *J. Comput. Phys.* 188 (1) (2003) 157–175.
- [3] X. Antoine, C. Besse, V. Mouysset, Numerical schemes for the simulation of the two-dimensional Schrödinger equation using non-reflecting boundary conditions, *Math. Comp.* 73 (248) (2004) 1779–1799 (electronic).
- [4] A. Bandrauk, *Molecules in Laser Fields*, M. Dekker, New York, 1994 (Chapter 1).
- [5] A. Bandrauk, S. Chelkowski, Dynamic imaging of nuclear wavefunctions with ultrashort UV laser pulses, *Phys. Rev. Lett.* 87 (27) (2001) 113–120.
- [6] A. Bandrauk, S. Chelkowski, S. Goudreau, *J. Mod. Opt.* 52 (411) (2005).
- [7] A. Bandrauk, S. Chelkowski, N.H. Shon, Nonlinear photon processes in molecules at high intensities—route to XUV-attosecond pulse generation, *J. Mol. Structure* 735–736 (2005) 203–209.
- [8] A. Bandrauk, S. Chelkowski, H. Yu, E. Constant, Enhanced harmonic generation in extended molecular systems by two-color excitation, *Phys. Rev. A* 56 (1997) 2537–2540.
- [9] L. Baudouin, O. Kavian, J.-P. Puel, Régularité dans une équation de Schrödinger avec potentiel singulier à distance finie et à l'infini, *C. R. Math. Acad. Sci. Paris* 337 (11) (2003) 705–710.
- [10] L. Baudouin, O. Kavian, J.-P. Puel, Regularity for a Schrödinger equation with singular potentials and application to bilinear optimal control, *J. Differential Equations* 216 (1) (2005) 188–222.
- [11] A. BenYedder, C. Le Bris, O. Atabek, A. Bandrauk, S. Chelkowski, Optimal control of attosecond pulse synthesis from high order harmonics generation, *Phys. Rev. A* 69 (041802) (2004).
- [12] C. Besse, B. Bidégaray-Fesquet, A. Bourgeade, P. Degond, O. Saut, A Maxwell–Bloch model with discrete symmetries for wave propagation in nonlinear crystals: an application to KDP, *M2AN Math. Model. Numer. Anal.* 38 (2) (2004) 321–344.
- [13] T. Brabec, F. Krausz, Intense few-cycle laser fields: frontier of nonlinear optics, *Rev. Mod. Phys.* 72 (545) (2000).
- [14] S. Chelkowski, A. Bandrauk, P.-B. Corkum, Femtosecond Coulomb explosion imaging of vibrational wave functions, *Phys. Rev. Lett.* 82 (17) (1999) 3416.
- [15] S. Chelkowski, C. Foisy, A. Bandrauk, Electron-nuclear dynamics of multiphoton H_2^+ dissociative ionization in intense laser fields, *Phys. Rev. A* 57 (2) (1998) 1176–1185.
- [16] I. Christov, Generation and propagation of attosecond X-ray pulses in gaseous media, *Phys. Rev. A* 57 (4) (1998) 2285–2288.
- [17] I. Christov, Enhanced generation of attosecond pulses in dispersion-controlled hollow-core fiber, *Phys. Rev. A* 60 (4) (1999) 3244–3250.
- [18] C. Cohen Tannoudji, J. Dupont-Roc, G. Grynberg, *Atom–Photon Interactions*, Wiley Interscience, New York, 1992.
- [19] P.-B. Corkum, Plasma perspective on strong-field multiphoton ionization, *Phys. Rev. Lett.* 71 (1993) 1994.
- [20] M. Defranceschi, C. Le Bris (Eds.), *Mathematical Models and Methods for Ab Initio Quantum Chemistry*, Lecture Notes in Chemistry, vol. 74, Springer-Verlag, Berlin, 2000.
- [21] E. Dumas, Global existence for Maxwell–Bloch systems, *J. Differential Equations* 219 (2) (2005) 484–509.
- [22] R.J. Iório Jr., D. Marchesin, On the Schrödinger equation with time-dependent electric fields, *Proc. Roy. Soc. Edinburgh Sect. A* 96 (1–2) (1984) 117–134.
- [23] J.-D. Jackson, *Classical Electrodynamics*, second ed., John Wiley & Sons Inc., New York, 1975.
- [24] C. Jungreuthmayer, M. Geissler, J. Zanghelini, T. Brabec, Microscopic analysis of large-cluster explosion in intense laser fields, *Phys. Rev. Lett.* 92 (13) (2004) 133401-1–133401-4.
- [25] M. Lewenstein, Ph. Balcou, M. Yu, A. Huillier, P.B. Corkum, Theory of high-harmonic generation by low frequency laser fields, *Phys. Rev. A* 49 (3) (1994) 2117–2132.
- [26] E. Lorin, S. Chelkowski, A. Bandrauk, Mathematical modeling of boundary conditions for laser–molecule TDSE and their numerical computation, *Numer. Methods Partial Differential Equations* (2007), submitted for publication.
- [27] E. Lorin, S. Chelkowski, A. Bandrauk, A Maxwell–Schrödinger model for non-perturbative laser–molecule interaction and some methods of numerical computation, *Proceeding CRM, High Partial Differential Equations in Science and Engineering*, vol. 41, American Mathematics Society, 2007, pp. 161–182.
- [28] E. Lorin, G. Zérah, A recursion method for the electronic structure calculation, *Comput. Phys. Comm.* 158 (1) (2004).
- [29] E. Lorin de la Grandmaison, S.B. Gowda, Y. Saad, M.L. Tiago, J.R. Chelikowsky, Efficient computation of the coupling matrix in time-dependent density functional theory, *Comput. Phys. Comm.* 167 (1) (2005) 7–22.
- [30] G. Mechain, A. Couairon, M. Franco, B. Prade, A. Mysyrowicz, Organizing multiple femtosecond filaments in air, *Phys. Rev. Lett.* 93 (3) (2004) 035003-1–035003-4.
- [31] G. Mur, Absorbing boundary conditions for the finite-difference approximation of the time-domain electromagnetic-field equations, *IEEE Trans. Electromagn. Compatibility EMC-23* (1981) 377–382.
- [32] S.C. Rae, K. Burnett, Harmonic generation and phase matching in the tunnelling limit, *J. Phys. B: At. Mol. Opt. Phys.* 26 (1993) 1509–1518.
- [33] S.C. Rae, K. Burnett, Phase matching of high-order harmonics in a rapidly ionizing medium, *Phys. Rev. A* (1994).
- [34] Y. Saad, W. Schultz, GMRES: a generalized minimal algorithm for solving nonsymmetric linear systems, *SIAM J. Sci. Statist. Comput.* 7 (3) (1986) 856–869.
- [35] O. Saut, Computational modeling of ultrashort powerful laser pulses in a nonlinear crystal, *J. Comp. Phys.* 197 (2) (2004) 624–646.
- [36] A. Schädle, Non-reflecting boundary conditions for the two-dimensional Schrödinger equation, *Wave Motion* 35 (2) (2002) 181–188.
- [37] N.-H. Shon, A. Suda, K. Midorikawa, Generation and propagation of attosecond pulses in the gas with sub-10-fs driver pulses, *Phys. Rev. A* 60 (3) (1999) 2587–2590.
- [38] A. Szabo, N.-S. Ostlünd, *Modern Quantum Chemistry: Introduction to Advanced Electronic Structure*, Dover Publications, Inc., 1996.
- [39] M.W. Walser, C.H. Keitel, A. Scrinzi, T. Brabec, High harmonic generation beyond the electric dipolar approximation, *Phys. Rev. Lett.* 85 (2000) 5082–5085.
- [40] K.S. Yee, Numerical solution of initial boundary value problems involving Maxwell's equations in isotropic media, *IEEE Trans. Antennas Propagation AP-16* (1966) 302–307.